Received 29 May 2024; revised 25 July 2024; accepted 20 August 2024. Date of publication 26 August 2024; date of current version 5 September 2024.

Digital Object Identifier 10.1109/OJCOMS.2024.3449701

Cooperative Bit Allocation in In-Band Full-Duplex Power Line Communication

VITALI KORZHUN (Graduate Student Member, IEEE), AND ANDREA M. TONELLO (Senior Member, IEEE)

Institute of Networked and Embedded Systems, University of Klagenfurt, 9020 Klagenfurt am Wörthersee, Austria

CORRESPONDING AUTHOR: V. KORZHUN (e-mail: vitali.korzhun@aau.at)

ABSTRACT In-band full-duplex (IBFD) is an attractive technology in broadband power line communication (BB-PLC) because it helps to improve spectral efficiency. However, IBFD is challenging since it requires additional hardware and advanced signal processing to mitigate self-interference (SI) signals. SI cancelation architectures and channel estimation techniques determine the overall IBFD performance. Accurate SI channel estimation is required since imperfect SI cancelation reduces signal-to-interference-plus-noise ratio (SINR), causing an increase in data errors and a decrease in data rates. Although channel estimation can be improved by sending additional training symbols, increasing the training duration will lower data throughput. Thus, the training symbol number is an essential trade-off for IBFD performance in BB-PLC. In this paper, we investigate IBFD performance in single-input single-output (SISO), single-input multiple-output (SIMO), and multiple-input multiple-output (MIMO) communication scenarios, including the influence of the training period. By analyzing error vectors on a constellation diagram, we obtain the closed-form expressions for the symbol error probability (SEP) affected by IBFD and the training duration. Based on the obtained expressions, we propose a bit allocation algorithm to determine bit loading to ensure reliable IBFD communication. Furthermore, we suggest a procedure to compute the optimal training symbol number that maximizes throughput in IBFD. Using the proposed bit allocation strategy and a database of measured channels, we estimated the achievable bidirectional throughput and the throughput gain in IBFD compared to time division duplexing (TDD).

INDEX TERMS In-band full-duplex, MIMO, power line communications, self-interference cancelation.

I. INTRODUCTION

BROADBAND Power Line Communication (BB-PLC) leverages the power line infrastructure for high-speed communication and is used in various outdoor and indoor applications. With growing data rates, coverage, and latency requirements, BB-PLC needs technologies to satisfy these ever-increasing demands. In-band full-duplex (IBFD) is a technology that allows to transmit and receive signals simultaneously on the same frequency band and in the same communication medium. Since neither time nor frequency separation is required, the bidirectional throughput of a system can, theoretically, be doubled. The interest in IBFD technology for BB-PLC started after some progress in the wireless domain [1], [2]. The first work about IBFD for BB-PLC was documented in [3], where the IBFD requirements and feasibility were studied. Unlike in wireless communications, where the self-interference (SI) power is typically more than 100 dB higher than the signal-of-interest (SOI) [4], IBFD in BB-PLC requires SI suppression to only up to 80 dB [3], which simplifies the SI cancelation architecture. For the SI mitigation, [3] proposed an architecture comprising two SI cancelation stages. In the first stage, a hybrid coupler was considered, which also received special attention in [5], [6] and was even physically realized in [7]. For the second stage, digital interference cancelation (DIC) and digitally assisted analog interference cancelation (AIC) were proposed and analyzed in [8] and [9].

From the channel estimation perspective, the SI and SOI channels must be accurately estimated to enable IBFD. The SI channel estimation, especially, requires very high accuracy because the imperfect SI estimation is projected onto a

higher residual SI (RSI) signal, resulting in a lower signal-to-interference-plus-noise ratio (SINR). Higher accuracy is achievable with a longer convergence time of adaptive algorithms or by utilizing more training symbols. The longer the channel estimation time, the lower the effective throughput. Additionally, BB-PLC has to cope with the linear periodically time-varying (LPTV) channel behavior, characterized by cyclic channel variations [10], [11]. This phenomenon requires either quick channel adaptation or complete channel re-estimation. The first option to cope with the LPTV channels was used in [8], [9] and the second one was considered in [12], [13]. Unfortunately, both solutions affect system throughput.

To address the adverse effect of LPTV channels, [8] proposed an LPTV-aware Least Mean Square (LMS) channel adaptation. Using this adaptation method, works [8] and [9] estimated the theoretical data rate gain (DRG) of IBFD over half-duplex (HDX) communication for single-input single-output (SISO) as well as for multiple-input multiple-output (MIMO) communication. However, DRG values presented in [8], [9] were obtained under the assumption that SI signals are suppressed to the level defined by the convergence of the LPTV-aware LMS algorithm. The LPTV-LMS convergence was reached by about 900 orthogonal frequency-division multiplexing (OFDM) symbols [8], which is significantly high and it lowers the practical value of the declared DRGs.

Alternatively, IBFD communication can be organized in time slots that do not exceed the channel coherence time and include the training period for independent SI and SOI channel estimation in the HDX mode. Such an approach increases the training period of IBFD by two times compared to time-division duplexing (TDD) but helps to achieve good initial channel estimation results. According to [13], training using two known OFDM symbols is sufficient to separately estimate the SI and SOI channels in SISO, SIMO, and MIMO. For all communication scenarios, [13] reported bidirectional throughput gain (BTG) from 1.79 to 1.88 in 2-30 MHz assuming a constant noise power spectral density (PSD) of -130 dBm/Hz. Since the noise PSD is frequency-dependent in BB-PLC, the reported BTGs may be over-optimistic. Then, computing realistic IBFD gains and throughput in BB-PLC remains an interesting objective.

A. RELATED WORK

Several studies have addressed the IBFD performance and bit allocation (BA) in the wireless domain and BB-PLC.

In wireless, [14] addressed bit and power allocation in a single-cell full-duplex (FDX) OFDMA network with one base station (BS) and multiple FDX mobile stations (MS). The work modeled RSI as an increase in noise level by a constant value. The goal was to maximize the sum-rate performance by optimizing the exclusive subcarrier assignment to the nodes under power restrictions for the BS and the MSs. Power allocation was performed by an iterative water-filling algorithm. The study showed a drop in IBFD DRGs from 99% to 47% as the RSI increased from 0 to 5 dB.

Another research in wireless [15] used stochastic geometry to analyze the FDX throughput improvement with imperfect SI cancelation. The effects of imperfect SI cancelation on the throughput were analyzed using the mathematical model. The research highlighted the important conclusion that there is a break-even point where the FDX and HDX throughputs are the same, and RSI determines the maximal distance within which FDX is beneficial over HDX.

A thorough analytical study was done by [16] aiming to maximize DRGs under non-negligible SI. It was proven (Lemma 1) that if FDX can outperform HDX for a given link, it is always optimal for the MS and the BS to transmit at their maximum allowed power. The numerical evaluations demonstrated the capacity gains in three different use cases.

In BB-PLC, the first results for IBFD throughput and DRGs were presented in [3] for SISO. BA was determined using look-up tables based on the SINR values affected by the ADC distortions. The DRGs were computed as the sum of allocated bits on the available subcarriers. This study continued in [8] and [9], where the DIC and AIC architectures were proposed. Using 1500 random simulated MIMO channels, the study declared a DRG of 2 for over 70% of the channels under a high noise level and a median gain of 1.8 under low noise levels using the AIC solution.

Another work in BB-PLC [13] performed Monte-Carlo simulations over 80 measured channels to estimate the achievable bidirectional throughput offered by IBFD in SISO, SIMO, and MIMO scenarios. Bit allocation was based on the SNR gap approach with the target symbol error probability (SEP) of 10^{-3}. Using two training OFDM symbols for independent SI and SOI channel estimation, the work achieved IBFD BTG varying from 1.79 to 1.88, with median values of 1.86 in SISO, 1.87 in SIMO, and 1.84 in MIMO. The reported median throughput in 2-30 MHz amounted to 300, 324, and 525 Mb/s in SISO, SIMO, and MIMO, respectively.

B. CONTRIBUTION AND OUTLINE

This paper aims to evaluate realistic IBFD performance gains considering channel estimation and bit allocation strategies. Peer-to-peer communication between two IBFD-capable nodes in a BB-PLC network is considered. Each transmission frame starts with a training sequence for channel estimation executed in the HDX mode, followed by the payload transmission either in the FDX or HDX. Upon the reception of channel state information from the opposite side, the communicating nodes can cooperatively switch between communication modes such as SISO TDD, SISO IBFD, SIMO TDD, SIMO IBFD, MIMO TDD, or MIMO IBFD, adjusting their BA appropriately. Moreover, the nodes can negotiate and adjust BA to enable asymmetric bidirectional throughput. The specific contributions are:

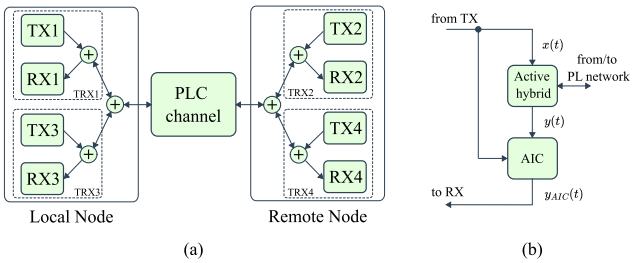

FIGURE 1. The system model for (a) 2x2 MIMO communication with (b) two-stage SI cancelation scheme.

- the characterization of SI and SOI channel estimation errors in SISO, SIMO, and MIMO, followed by the derivation of SEPs in IBFD with the dependence on the training period duration;
- the proposal of a novel bit allocation scheme for reliable IBFD communication, considering a subroutine to compute the optimal training symbol number;
- the estimation of realistic bidirectional throughput and IBFD gain in BB-PLC using the proposed BA.

The rest of the paper is organized as follows. The system model of the IBFD system in general MIMO configuration is presented in Section II. IBFD performance metrics are discussed in Section III. Section IV derives the closed-form expressions for SEPs in all communication modes. Section V presents our BA algorithm, which was numerically analyzed over BB-PLC channels and used to estimate IBFD BTGs in Section VI. Finally, Section VII concludes this paper.

II. SYSTEM MODEL

Two nodes, shown in Fig. 1a as the Local Node (LN) and Remote Node (RN), communicate with each other through IBFD or TDD. Each node has two transmitters (TX) and two receivers (RX) and can support SISO, 1x2 SIMO, or 2x2 MIMO communication. In any communication scenario, the signal at the receiver j is given in the time domain (TD) by

$$y_j(t) = \sum_{i=1}^{N_{TX}} x_i * h_{ij}(t) + w_j(t), \tag{1}$$

where N_{TX} is the number of operating transmitters, both local and remote, $x_i(t)$ is the signal sent by the i-th transmitter, $h_{ij}(t)$ is the channel impulse response that describes the channel link between the i-th TX and j-th RX, and $w_j(t)$ is the noise measured at the receiver.

To enable IBFD communication, the SI signals must be suppressed. The SI cancelation in each transceiver is executed in a two-stage cancelation scheme depicted in Fig. 1b. The initial cancelation is made by an active hybrid, which prevents signal propagation from a transmitter path chain to a receiver path chain. The second stage is AIC, the analog interference cancelation. AIC aims to estimate the SI signals after active hybrid, synthesize the SI signal replicas, and eventually cancel the SI signals in the analog domain. In MIMO, each AIC module synthesizes two replicas to cancel two SI signals as

$$y_{AIC_j}(t) = y_j(t) - \sum_{i \in SI} x_i * \hat{h}_{ij}(t), \tag{2}$$

where $\hat{h}_{ij}$ is the estimate of the channel impulse response h_{ij}.

Since BB-PLC utilizes OFDM symbols, it is convenient to represent the system model in the frequency domain (FD) independently for each subchannel (subcarrier). Then, the LN is described at the active hybrids and the AICs in the FD as

$$\begin{bmatrix} Y_1 \\ Y_3 \end{bmatrix} = \begin{bmatrix} H_{11} & H_{31} \\ H_{13} & H_{33} \end{bmatrix} \cdot \begin{bmatrix} X_1 \\ X_3 \end{bmatrix} + \begin{bmatrix} H_{21} & H_{41} \\ H_{23} & H_{43} \end{bmatrix} \cdot \begin{bmatrix} X_2 \\ X_4 \end{bmatrix} + \begin{bmatrix} W_1 \\ W_3 \end{bmatrix}, \tag{3}$$

$$\begin{bmatrix} Y_{AIC1} \\ Y_{AIC3} \end{bmatrix} = \begin{bmatrix} E_{AIC1} \\ E_{AIC3} \end{bmatrix} + \begin{bmatrix} H_{21} & H_{41} \\ H_{23} & H_{43} \end{bmatrix} \cdot \begin{bmatrix} X_2 \\ X_4 \end{bmatrix} + \begin{bmatrix} W_1 \\ W_3 \end{bmatrix}, \tag{4}$$

where Y is the measured signal, X is the M-QAM-modulated transmitted signal, H is the channel attenuation at a given frequency, and W is the aggregated noise. The term E_{AIC} represents an RSI signal. The RSI at the LN is given by

$$\begin{bmatrix} E_{AIC1} \\ E_{AIC3} \end{bmatrix} = \begin{bmatrix} H_{11} & H_{31} \\ H_{13} & H_{33} \end{bmatrix} \cdot \begin{bmatrix} X_1 \\ X_3 \end{bmatrix} - \begin{bmatrix} \hat{H}_{11} & \hat{H}_{31} \\ \hat{H}_{13} & \hat{H}_{33} \end{bmatrix} \cdot \begin{bmatrix} X_1 \\ X_3 \end{bmatrix}. \tag{5}$$

Similarly, the RN is represented at each subcarrier by

$$\begin{bmatrix} Y_2 \\ Y_4 \end{bmatrix} = \begin{bmatrix} H_{12} & H_{32} \\ H_{14} & H_{34} \end{bmatrix} \cdot \begin{bmatrix} X_1 \\ X_3 \end{bmatrix} + \begin{bmatrix} H_{22} & H_{42} \\ H_{24} & H_{44} \end{bmatrix} \cdot \begin{bmatrix} X_2 \\ X_4 \end{bmatrix} + \begin{bmatrix} W_2 \\ W_4 \end{bmatrix}, \tag{6}$$

$$\begin{bmatrix} Y_{AIC2} \\ Y_{AIC4} \end{bmatrix} = \begin{bmatrix} H_{12} & H_{32} \\ H_{14} & H_{34} \end{bmatrix} \cdot \begin{bmatrix} X_1 \\ X_3 \end{bmatrix} + \begin{bmatrix} E_{AIC2} \\ E_{AIC4} \end{bmatrix} + \begin{bmatrix} W_2 \\ W_4 \end{bmatrix}. \tag{7}$$

A. CHANNEL ESTIMATION

A BB-PLC channel can abruptly change its characteristics, such as the channel response and the noise profile, with respect to the mains cycle phase. However, it can be considered static between changes and periodic, as shown in Fig. 2a. Reliable communication can be executed within stationary periods. For robustness, N_T training OFDM symbols with block-type pilot insertion precede N_P payload OFDM symbols in each transmission frame. For accurate SI and SOI channel estimation in IBFD, each of the nodes transmits the training OFDM symbols separately in the HDX mode, as shown in Fig. 2c, making IBFD channel estimation twice as long compared to TDD (see Fig. 2b).

In SISO and SIMO, channel estimation is performed using the Least Square (LS) method utilizing known 4-QAM training symbols X_T independently at each subcarrier:

$$Y = H \cdot X_T + W, \tag{8}$$

$$\hat{H} = Y \cdot X_T^{-1} = H + W \cdot X_T^{-1}. \tag{9}$$

Using N_T training OFDM symbols, we obtain N_T channel estimates per subcarrier given by (9) that can be averaged to improve accuracy as follows

$$\hat{H} = \frac{1}{N_T} \sum_{l=0}^{N_T-1} Y^{(l)} \cdot \left(X_T^{(l)}\right)^{-1}. \tag{10}$$

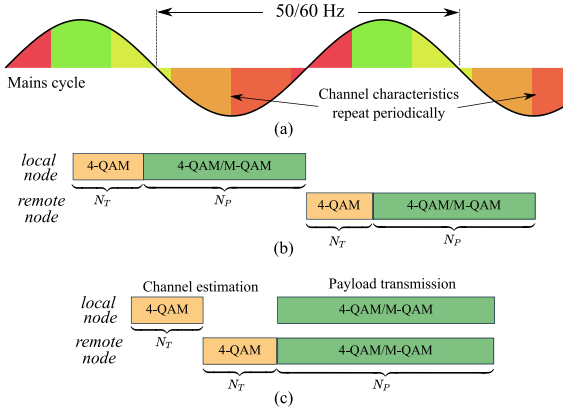

FIGURE 2. LPTV channel (a) and transmission frames in (b) TDD and (c) IBFD communication with N_T training and N_P payload OFDM symbols.

TABLE 1. Pattern of orthogonal symbols for channel initialization in the half-duplex mode.

OFDM:	0	1	2	3	4	5	6	7
TX1 (TX2)	1	1	-1	-1	1	1	-1	-1
TX3 (TX4)	1	-1	-1	1	1	-1	-1	1

Channel estimation in MIMO differs from SISO and SIMO channel estimation. Two consecutive training OFDM symbols sent by two transmitters form an orthogonal 2x2 Hadamard matrix at each subcarrier. From (3)-(4), SI and SOI channel estimates for the LN can be found as

$$\begin{bmatrix} \hat{H}_{11}^{(l)} & \hat{H}_{31}^{(l)} \\ \hat{H}_{13}^{(l)} & \hat{H}_{33}^{(l)} \end{bmatrix} = \begin{bmatrix} Y_{AIC1}^{(l-1)} & Y_{AIC1}^{(l)} \\ Y_{AIC3}^{(l-1)} & Y_{AIC3}^{(l)} \end{bmatrix} \cdot \begin{bmatrix} X_1^{(l-1)} & X_1^{(l)} \\ X_3^{(l-1)} & X_3^{(l)} \end{bmatrix}^{-1}, \quad (11)$$

$$\begin{bmatrix} \hat{H}_{21}^{(l)} & \hat{H}_{41}^{(l)} \\ \hat{H}_{23}^{(l)} & \hat{H}_{43}^{(l)} \end{bmatrix} = \begin{bmatrix} Y_{AIC1}^{(l-1)} & Y_{AIC1}^{(l)} \\ Y_{AIC3}^{(l-1)} & Y_{AIC3}^{(l)} \end{bmatrix} \cdot \begin{bmatrix} X_2^{(l-1)} & X_2^{(l)} \\ X_4^{(l-1)} & X_4^{(l)} \end{bmatrix}^{-1}. \quad (12)$$

To perform MIMO channel estimation over N_T training symbols, we use orthogonal pairs created from the pattern shown in Table 1. This repetitive pattern guarantees orthogonality for any two consecutive symbols and can be adjusted to any training period duration. Particularly, the first two training pairs and their inverse are

$$\begin{bmatrix} X_1^{(0)} & X_1^{(1)} \\ X_3^{(0)} & X_3^{(1)} \end{bmatrix} = X_T \begin{bmatrix} 1 & 1 \\ 1 & -1 \end{bmatrix}, \begin{bmatrix} X_1^{(0)} & X_1^{(1)} \\ X_3^{(0)} & X_3^{(1)} \end{bmatrix}^{-1} = \frac{1}{2X_T} \begin{bmatrix} 1 & 1 \\ 1 & -1 \end{bmatrix}, \quad (13)$$

where X_T is a known 4-QAM symbol.

Using N_T training symbols, we generate N_T-1 orthogonal pairs and obtain N_T-1 channel estimates. By averaging, we improve the accuracy of SI and SOI channel estimation as

$$\begin{bmatrix} \hat{H}_{11} & \hat{H}_{31} \\ \hat{H}_{13} & \hat{H}_{33} \end{bmatrix} = \frac{1}{N_T-1} \sum_{l=1}^{N_T-1} \begin{bmatrix} \hat{H}_{11}^{(l)} & \hat{H}_{31}^{(l)} \\ \hat{H}_{13}^{(l)} & \hat{H}_{33}^{(l)} \end{bmatrix}, \quad (14)$$

$$\begin{bmatrix} \hat{H}_{21} & \hat{H}_{41} \\ \hat{H}_{23} & \hat{H}_{43} \end{bmatrix} = \frac{1}{N_T-1} \sum_{l=1}^{N_T-1} \begin{bmatrix} \hat{H}_{21}^{(l)} & \hat{H}_{41}^{(l)} \\ \hat{H}_{23}^{(l)} & \hat{H}_{43}^{(l)} \end{bmatrix}. \quad (15)$$

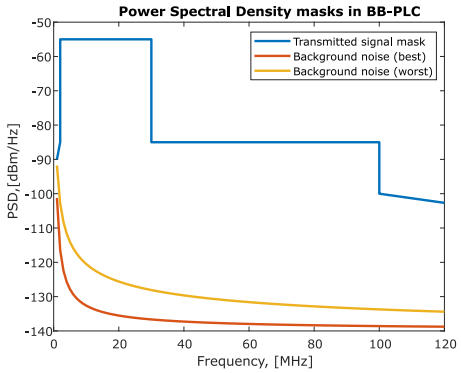

FIGURE 3. The PSD mask for transmitted signal and models for the background noise.

B. POWER SPECTRAL DENSITY (PSD)

In BB-PLC, the transmission power is limited, and the PSD mask is applied to avoid interference to other systems. The PSD mask specified by the G.hn standard [17] is frequency dependent, as shown in Fig. 3. Thus, a transmitted symbol X can be generated with specific power requirements and modulation as follows

$$X = \sqrt{E_S} \frac{S}{||S||} = \sqrt{E_S} \frac{S_I + jS_Q}{\sqrt{\bar{E}_M}}, \quad (16)$$

where E_S is the frequency-dependent average power of the transmitted symbol, and $\bar{E}_M$ is the average power of the associated constellation points for a given M-QAM.

In a square M-QAM, the constellation points have the in-phase $S_I=2i-\sqrt{M}-1$ and the quadrature $S_Q=2q-\sqrt{M}-1$ components with $i, q \in \{1, \ldots, \sqrt{M}\}$. Then, the M-QAM average power is equal to

$$\bar{E}_M = \frac{1}{M} \sum_{i=1}^{\sqrt{M}} \sum_{q=1}^{\sqrt{M}} S_I^2 + S_Q^2 = \frac{2}{3}(M-1). \quad (17)$$

A BB-PLC network is exposed to different noise types. Overall, the superposition of noise components yields background noise with a complex-shaped PSD profile, as illustrated in [18, Fig. 9]. For the objectives of this paper, the PSD of the cumulative noise W in (8) can be modeled with a simplified frequency-dependent model defined in [18], [19] and given by

$$R_W(f) = a + bf^c \quad \left[\frac{\text{dBm}}{\text{Hz}}\right], \quad (18)$$

where f is the frequency in MHz and the parameters $(a, b, c) = (-145, 53.23, -0.337)$ describe the worst noise scenario and the coefficients $(a, b, c) = (-140, 38.75, -0.72)$ describe the best noise conditions.

III. IBFD PERFORMANCE METRICS

In the IBFD BB-PLC literature, DRG in [3], [8], [9] and BTG in [13] were considered as the performance metrics to compare IBFD and TDD. Since DRG does not include the time spent on channel estimation, which can severely

downgrade the system throughput, we will use only BTG as the IBFD performance metric in this article.

We define the bidirectional throughput gain as

$$BTG = \frac{BT^{(IBFD)}}{BT^{(TDD)}} = \frac{T_{LN}^{(IBFD)} + T_{RN}^{(IBFD)}}{\frac{1}{2}\left(T_{LN}^{(TDD)} + T_{RN}^{(TDD)}\right)}, \tag{19}$$

where T_{LN} and T_{RN} are the total achievable throughput for the local and the remote nodes, respectively.

The data throughput in *bits/s* at a given transmitter is computed as follows

$$T = \rho \frac{C\left(1 - \bar{P}_b\right)}{T_s}, \tag{20}$$

where ρ is the coefficient that characterizes the proportion of OFDM symbols with payload, C is the number of bits carried by one OFDM symbol, $\bar{P}_b$ is the average bit error probability, and T_s is the duration of one OFDM symbol. Assuming independent M-QAM bit allocation for each subcarrier, C can be computed as

$$C = \sum_{k=1}^{N_{asc}} n_k = \sum_{k=1}^{N_{asc}} \log_2 M_k, \tag{21}$$

where N_{asc} is the number of active subcarriers and n_k is the number of bits loaded on the k-th subcarrier. Bit allocation n_k can be determined by the SNR gap approach [13], [20], [21] as follows

$$n_k \le \log_2\left(1 + \frac{\mathsf{SINR}_k}{\Gamma}\right), \tag{22}$$

where Γ is the SNR gap computed for a given symbol error threshold P_0 as

$$\Gamma = \frac{1}{3}\left[Q^{-1}\left(\frac{P_0}{4}\right)\right]^2, \tag{23}$$

where Q^{-1} is the inverse of $Q(x) = \frac{1}{\sqrt{2\pi}} \int_x^\infty e^{-t^2} dt$.

From Fig. 2, the coefficient ρ is calculated for TDD and IBFD as

$$\rho_{TDD} = \frac{N_P}{N_P + N_T} = 1 - \frac{N_T}{N_{CT}}, \tag{24}$$

$$\rho_{IBFD} = \frac{N_P}{N_P + 2N_T} = 1 - \frac{2N_T}{N_{CT}}, \tag{25}$$

where N_P is the number of payload symbols, and N_{CT} is the total number of OFDM symbols that can be delivered within the channel coherence time or limited by the transmission frame duration.

According to [13, Fig. 4], C in (20) is monotonically increasing with the increase of N_T. Since $\rho(N_T)$ is linearly decreasing, there is the optimal training symbol number N_T^{opt}, where the throughput T reaches its maximum. N_T^{opt} in [13] differs for duplexing (IBFD or TDD), channel realizations, and communication modes. The observed dependency $C(N_T)$ anticipates the dependence of SINR on N_T, and obtaining analytic expressions for it in different modes is desirable to select an optimal N_T and achieve the best IBFD performance.

Computing $\bar{P}_b$ in (20) can be done based on the analysis of bit error probability (BEP) P_b or symbol error probability (SEP) P_s over all subcarriers. A closed-form expression of BEP P_b for M-QAM over an additive white Gaussian noise (AWGN) channel is known from [22], while SEP P_s for M-QAM over an AWGN channel is defined in [23] as

$$P_s = 4\left(1 - \frac{1}{\sqrt{M}}\right) Q\left(\sqrt{\frac{3}{M-1}\bar{\gamma}}\right) - 4\left(1 - \frac{1}{\sqrt{M}}\right)^2 Q^2\left(\sqrt{\frac{3}{M-1}\bar{\gamma}}\right), \tag{26}$$

where M is the applied modulation order and $\bar{\gamma}$ is the average SNR per symbol.

For IBFD BB-PLC, P_s (P_b) requires further analysis because P_s is a function of SINR, which is expected to be influenced by N_T. Considering also channel estimation errors, the distribution of the resulting noise on a constellation plot might not be Gaussian and (26) may not be directly usable. Furthermore, the common assumption that symbol error occurs only at the closest neighboring symbols, affecting only 1 bit in the Gray coding scheme, may not be applicable in IBFD communication. Thus, considering $P_b \ge \frac{P_s}{\log_2 M}$, the average BEP $\bar{P}_b$ shall be expressed as the following bound

$$\bar{P}_b = \frac{N_{err}}{C} \ge \frac{\sum_{k=1}^{N_{asc}} 1 \cdot P_s(\gamma_k, M_k, N_T)}{C} = \frac{\sum_{k=1}^{N_{asc}} P_s(\gamma_k, M_k, N_T)}{\sum_{k=1}^{N_{asc}} \log_2 M_k}, \tag{27}$$

where N_{err} is the expected number of bit errors per OFDM symbol. $P_s(\gamma_k, M_k, N_T)$ as a function of the relevant parameters will be determined in Section IV.

Consequently, the upper bound on the data throughput defined in (20) for a given transmitter is estimated by

$$T \le \frac{\rho}{T_s} \sum_{k=1}^{N_{asc}} \left(\log_2 M_k - P_s(\gamma_k, M_k, N_T)\right). \tag{28}$$

To achieve the highest IBFD performance, we must determine not only the bit allocation but also the number of training symbols N_T that maximizes the throughput for both nodes under the presence of interference. Assuming $n_{i,k}$ is the number of bits allocated by the i-th transmitter at the k-th subcarrier, the maximization of the bidirectional throughput (the upper bound) in IBFD can be formulated as the following optimization problem

$$\begin{aligned} \underset{N_T,\, n_{i,k}}{\text{maximize}} \quad & \frac{\rho(N_T)}{T_s} \sum_{i=1}^{N_{TX}} \sum_{k=1}^{N_{asc}} \left(n_{i,k} - P_s\left(\gamma_{i,k}, M_{i,k}, N_T\right)\right) \\ \text{subject to} \quad & N_T > 0, \; N_T \in \mathbb{Z}, \\ & n_{i,k} \in \{0, 2, 4, 6, 8, 10\}, \\ & P_s\left(\gamma_{i,k}, M_{i,k}, N_T\right) \le P_0 \quad \forall i, k, N_T, \end{aligned} \tag{29}$$

where N_{TX} is the number of involved transmitters (2 in SISO or SIMO, and 4 in MIMO), $\gamma_{i,k}$ is the SNR at the

destination side for a signal from the i-th transmitter at the k-th subcarrier, and P_0 is the highest acceptable SEP.

The solution for this problem is in Section V.

IV. SYMBOL ERROR PROBABILITY

In this section, we investigate the influence of channel estimation on received symbols in a constellation. We derive the expressions for symbol error probability as a function of the training symbol number and the applied modulation.

A. DETERMINISTIC CHARACTERIZATION OF ERROR VECTORS IN IBFD

Let's consider SISO IBFD communication, where a node simultaneously receives a symbol X_{SOI} and transmits a symbol X_{SI}. The system model in (3)-(7) is simplified regardless of the considered node to the following equations

$$Y = H_{SI}X_{SI} + H_{SOI}X_{SOI} + W, \tag{30}$$

$$Y_{AIC} = Y - \hat{H}_{SI}X_{SI}, \tag{31}$$

$$Y_{AIC} = \left(H_{SI} - \hat{H}_{SI}\right)X_{SI} + H_{SOI}X_{SOI} + W. \tag{32}$$

Assuming sufficient SI cancelation, data symbols can be estimated as

$$\hat{X}_{SOI} = \hat{H}_{SOI}^{-1}Y_{AIC}. \tag{33}$$

Let $\Delta H_{SOI} \triangleq H_{SOI} - \hat{H}_{SOI}$ and $\Delta H_{SI} \triangleq H_{SI} - \hat{H}_{SI}$ be the estimation errors, describing the differences between actual channels H_{SI} and H_{SOI} and their estimations $\hat{H}_{SI}$ and $\hat{H}_{SOI}$. Then, after making some manipulations, we obtain

$$\begin{aligned}\hat{X}_{SOI} &= \hat{H}_{SOI}^{-1}\Big(\left(H_{SI} - \hat{H}_{SI}\right)X_{SI} + H_{SOI}X_{SOI} + W\Big)\\ &= \hat{H}_{SOI}^{-1}\Big(\Delta H_{SI}X_{SI} + \left(\Delta H_{SOI} + \hat{H}_{SOI}\right)X_{SOI} + W\Big)\\ &= X_{SOI} + \hat{H}_{SOI}^{-1}(\Delta H_{SI}X_{SI} + \Delta H_{SOI}X_{SOI} + W).\end{aligned} \tag{34}$$

Then, the error vector in the received data is given by

$$\Delta X_{SOI} = \hat{H}_{SOI}^{-1}(\Delta H_{SI}X_{SI} + \Delta H_{SOI}X_{SOI} + W). \tag{35}$$

From (35), three components contribute to errors in the received data signal. The error vector ΔX_{SOI} (see Fig. 4) consists of the SI and SOI channel estimation penalties, the transformed (amplified) background noise and is given by

$$\Delta X_{SOI} = E_{SI} + E_{SOI} + E_W, \tag{36}$$

where

$$E_{SI} = \hat{H}_{SOI}^{-1}\Delta H_{SI}X_{SI}, \tag{37}$$

$$E_{SOI} = \hat{H}_{SOI}^{-1}\Delta H_{SOI}X_{SOI}, \tag{38}$$

$$E_W = \hat{H}_{SOI}^{-1}W. \tag{39}$$

The components E_{SI} and E_{SOI} in (36) require special attention. They cannot be neglected but can be influenced by channel estimation. Moreover, they will contribute to data errors differently after changing modulation from 4-QAM to a higher order modulation due to the variation of the instant power in X_{SOI} and X_{SI}. Finally, E_{SI} is the component that distinguishes IBFD from TDD.

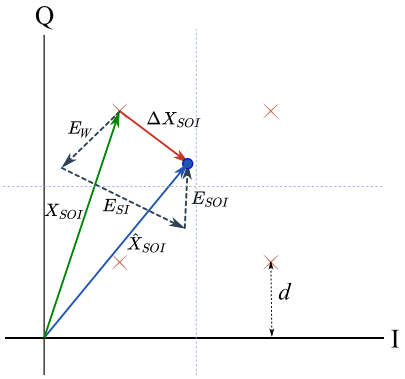

FIGURE 4. The components of the error vector on a constellation diagram.

As seen in Appendix A and B, error vectors in SIMO and MIMO IBFD communication can also be decomposed into three components.

B. STATISTICAL CHARACTERIZATION OF ERROR VECTORS IN IBFD

E_{SI} and E_{SOI} in (36) are characterized by the channel estimation errors ΔH_{SI} and ΔH_{SOI}, as well as the data symbols X_{SI} and X_{SOI}, which depend on the applied power E_S and the modulation order. ΔH_{SI} and ΔH_{SOI} are determined by channel estimation over N_T training symbols (see Fig. 2) and remain constant over the following N_P OFDM payload symbols if a channel is static and no channel tracking is applied. However, if we collect error vector measurements over many transmission frames such that the number of accumulated OFDM symbols $L \gg N_P$, we can characterize ΔX_{SOI} statistically. For further analysis, we assume all channels are static, and the cumulative noise W exhibits a normal distribution with $W \sim \mathcal{CN}(0, \sigma^2)$. Additionally, we assume that the nodes employ 4-QAM for channel estimation as well as for data transmission.

In SISO, the components ΔH_{SI} and ΔH_{SOI} are determined by channel estimation over N_T training symbols X_T. Then, from (9) and (10)

$$\Delta H_{SI} = \frac{1}{N_T}\sum_{i=0}^{N_T-1} -\frac{W^{(i)}}{X_T^{(i)}}, \quad \Delta H_{SOI} = \frac{1}{N_T}\sum_{i=0}^{N_T-1} -\frac{W^{(i)}}{X_T^{(i)}}. \tag{40}$$

Consequently, both ΔH_{SI} and ΔH_{SOI} are the averaged sums of noise samples but taken in different channel estimation phases, as shown in Fig. 2. Therefore, ΔH_{SI} and ΔH_{SOI} are independent and identically distributed (i.i.d.) random variables (RVs) with zero means and the variances given by

$$\mathbb{V}[\Delta H_{SI}] = \frac{\sigma^2}{N_T E_S}, \quad \mathbb{V}[\Delta H_{SOI}] = \frac{\sigma^2}{N_T E_S}. \tag{41}$$

The RV $\Delta X_{SOI} = E_{SI} + E_{SOI} + E_W$ is the sum of independent random variables. Therefore, the second moment (power) of the RV ΔX_{SOI} can be found as

$$\mathbb{E}\Big[|\Delta X_{SOI}|^2\Big] = \mathbb{E}\Big[|E_{SI}|^2\Big] + \mathbb{E}\Big[|E_{SOI}|^2\Big] + \mathbb{E}\Big[|E_W|^2\Big]. \quad (42)$$

Using the simplification $\hat{H}_{SOI}^{-1} \approx 1/H_{SOI}$, we can estimate all components in (42) as

$$\mathbb{E}\Big[|E_{SI}|^2\Big] = \mathbb{E}\left[\left(\frac{\Delta H_{SI} X_{SI}}{H_{SOI}}\right)\left(\frac{\Delta H_{SI} X_{SI}}{H_{SOI}}\right)^*\right] = \frac{\mathbb{E}\big[|\Delta H_{SI}|^2\big]\mathbb{E}\big[|X_{SI}|^2\big]}{|H_{SOI}|^2} = \frac{\sigma^2 E_S}{N_T E_S |H_{SOI}|^2} = \frac{\sigma^2}{N_T |H_{SOI}|^2}, \quad (43)$$

$$\mathbb{E}\Big[|E_{SOI}|^2\Big] = \mathbb{E}\left[\left(\frac{\Delta H_{SOI} X_{SOI}}{H_{SOI}}\right)\left(\frac{\Delta H_{SOI} X_{SOI}}{H_{SOI}}\right)^*\right] = \frac{\mathbb{E}\big[|\Delta H_{SOI}|^2\big]\mathbb{E}\big[|X_{SOI}|^2\big]}{|H_{SOI}|^2} = \frac{\sigma^2}{N_T |H_{SOI}|^2}, \quad (44)$$

$$\mathbb{E}\Big[|E_W|^2\Big] = \mathbb{E}\left[\left(\frac{W}{\hat{H}_{SOI}}\right)\left(\frac{W}{\hat{H}_{SOI}}\right)^*\right] = \frac{\sigma^2}{|H_{SOI}|^2}. \quad (45)$$

Since ΔX_{SOI} is a zero-mean RV, its variance from (42)-(46) is given by

$$\mathbb{V}[\Delta X_{SOI}] = \mathbb{E}\Big[|\Delta X_{SOI}|^2\Big] = \frac{\sigma^2}{|H_{SOI}|^2}\left(\frac{2}{N_T} + 1\right). \quad (46)$$

Similarly, the variances of ΔX_{SOI} in SIMO and MIMO IBFD are characterized in Appendix C and D.

From (46), we can find the SINR in SISO IBFD exploiting 4-QAM in both directions

$$\mathsf{SINR} = \frac{E_S}{\sigma^2}|H_{SOI}|^2\left(\frac{N_T}{N_T + 2}\right). \quad (47)$$

The SINR can be factorized in any communication scenario as $\mathsf{SINR} = \eta\ \gamma$, where γ is the real SNR at the receiver side offered by a channel, and η is the SNR degradation factor associated with channel estimation errors. SNR γ depends on the signal transmission power, the noise power, channel gains, and channel equalization techniques. SNR γ for all data symbols is presented in Table 2. The factor η depends on the duplexing mode (IBFD or TDD) and the training symbol number N_T. In IBFD, the factor η decreases compared to TDD due to additional SI channel estimation errors. The factor η is defined for 4-QAM in all the analyzed communication modes in Table 3.

C. ERROR PROBABILITY FOR M-QAM IN SISO IBFD

In a general M-QAM transmission, symbols are transmitted with varying instantaneous power, affecting the SI and SOI channel estimation errors in (37) and (38) and their statistical properties in (43) and (44). Thus, the instantaneous power of SI and SOI symbols must be considered in the derivation of SEPs. In this section, we derive the SEP in SISO IBFD.

A symbol error occurs if the error vector ΔX_{SOI} crosses inter-symbol decision boundaries. As shown in Fig. 4, all symbols in a square M-QAM constellation can be classified into three categories: symbols at the corners with two boundaries, symbols at the edges (three boundaries), and inner symbols surrounded by four decision boundaries. Symbols at corners and edges (both SOI and SI) are transmitted with a higher power, increasing the variance of ΔX_{SOI} and, consequently, the probability of a symbol error.

Let $X_{SOI}^{(i)}$, $i \in \{1, M_{SOI}\}$ and $X_{SI}^{(j)}$, $j \in \{1, M_{SI}\}$ be M-QAM signals with the modulation orders M_{SOI} and M_{SI}, respectively. If the power of the transmitted signals $|X_{SOI}^{(i)}|^2 = E_S \phi_i$ and $|X_{SI}^{(j)}|^2 = E_S \varphi_j$, then the effective variance of ΔX_{SOI} can be expressed in SISO IBFD as

$$\sigma_{ij}^2 = \mathbb{V}\Big[\Delta X_{SOI} | X_{SOI}^{(i)}, X_{SI}^{(j)}\Big] = \frac{\sigma^2}{|H_{SOI}|^2}\left(\frac{\phi_i + \varphi_j}{N_T} + 1\right), \quad (48)$$

where ϕ and φ are the normalized SOI and SI signal powers.

In general, SEP can be found as

$$P_s = \sum_{i=1}^{M_{SOI}} \sum_{j=1}^{M_{SI}} \mathbb{P}\Big[X_{SOI}^{(i)}\Big] \cdot \mathbb{P}\Big[X_{SI}^{(j)}\Big] \cdot \mathbb{P}\Big[Err | X_{SOI}^{(i)}, X_{SI}^{(j)}\Big]. \quad (49)$$

Assuming equiprobable symbols, we obtain

$$P_s = \frac{1}{M_{SOI} M_{SI}} \sum_{j=1}^{M_{SI}} \left(\sum_{i \in Corners} \mathbb{P}\Big[Err | X_{SOI}^{(i)}, X_{SI}^{(j)}\Big] + \sum_{i \in Edges} \mathbb{P}\Big[Err | X_{SOI}^{(i)}, X_{SI}^{(j)}\Big] \right.$$

TABLE 2. SNR at the destination side γ for different received symbols X_n in SISO, SIMO, and MIMO communications.

γ	SISO	SIMO	MIMO
X_1	$\frac{E_S}{\sigma^2}\lvert H_{12}\rvert^2$ $\frac{E_S}{\sigma^2}\lvert H_{14}\rvert^2$	$\frac{E_S}{\sigma^2}\left(\lvert H_{12}\rvert^2 + \lvert H_{14}\rvert^2\right)$	$\frac{E_S}{2\sigma^2}\frac{\lvert H_{34}H_{12} - H_{32}H_{14}\rvert^2}{\lvert H_{32}\rvert^2 + \lvert H_{34}\rvert^2}$
X_2	$\frac{E_S}{\sigma^2}\lvert H_{21}\rvert^2$ $\frac{E_S}{\sigma^2}\lvert H_{23}\rvert^2$	$\frac{E_S}{\sigma^2}\left(\lvert H_{21}\rvert^2 + \lvert H_{23}\rvert^2\right)$	$\frac{E_S}{2\sigma^2}\frac{\lvert H_{43}H_{21} - H_{23}H_{41}\rvert^2}{\lvert H_{43}\rvert^2 + \lvert H_{41}\rvert^2}$
X_3	$\frac{E_S}{\sigma^2}\lvert H_{32}\rvert^2$ $\frac{E_S}{\sigma^2}\lvert H_{34}\rvert^2$	$\frac{E_S}{\sigma^2}\left(\lvert H_{32}\rvert^2 + \lvert H_{34}\rvert^2\right)$	$\frac{E_S}{2\sigma^2}\frac{\lvert H_{34}H_{12} - H_{32}H_{14}\rvert^2}{\lvert H_{12}\rvert^2 + \lvert H_{14}\rvert^2}$
X_4	$\frac{E_S}{\sigma^2}\lvert H_{41}\rvert^2$ $\frac{E_S}{\sigma^2}\lvert H_{43}\rvert^2$	$\frac{E_S}{\sigma^2}\left(\lvert H_{41}\rvert^2 + \lvert H_{43}\rvert^2\right)$	$\frac{E_S}{2\sigma^2}\frac{\lvert H_{43}H_{21} - H_{23}H_{41}\rvert^2}{\lvert H_{23}\rvert^2 + \lvert H_{21}\rvert^2}$

TABLE 3. SNR degradation η for TDD and IBFD in SISO, SIMO, and MIMO.

η	SISO	SIMO	MIMO
IBFD	$\frac{N_T}{N_T+2}$	$\frac{N_T}{N_T+2}$	$\frac{N_T-1}{N_T+1}$
TDD	$\frac{N_T}{N_T+1}$	$\frac{N_T}{N_T+1}$	$\frac{N_T-1}{N_T}$

$$+\sum_{i\in Inners}\mathbb{P}\Big[Err|X_{SOI}^{(i)},X_{SI}^{(j)}\Big]\Bigg). \quad (50)$$

An error can occur if the component ΔX_{SOI} along in-phase or quadrature phase is greater than the distance d, resulting in $P_e^I=\mathbb{P}[\Re\{\Delta X_{SOI}\}>d]$ and $P_e^Q=\mathbb{P}[\Im\{\Delta X_{SOI}\}>d]$. Since the two phases are uncorrelated, their conditional variances are $\sigma_{ij}^2/2$, and the probability of crossing one decision border in any of the phases equals

$$P_e^I=P_e^Q=Q\left(\frac{d\sqrt{2}}{\sigma_{ij}}\right)=Q\left(\sqrt{\frac{3}{M_{SOI}-1}\frac{E_S}{\sigma_{ij}^2}}\right), \quad (51)$$

where

$$d=\frac{\sqrt{E_S}}{\sqrt{\frac{2}{3}(M_{SOI}-1)}}. \quad (52)$$

The correct decision is made if none of the decision boundaries in both dimensions is crossed: $P_c=(1-P_e^I)(1-P_e^Q)$. For each symbol category, we can find the error probability as

$$\mathbb{P}\Big[Err|X_{SOI}^{(i)},X_{SI}^{(j)}\Big]=\begin{cases}2Q-Q^2, & \text{if } i\in Corners\\ 3Q-2Q^2, & \text{if } i\in Edges\\ 4Q-4Q^2, & \text{if } i\in Inners\end{cases} \quad (53)$$

where Q denotes $Q(\sqrt{\frac{3}{M_{SOI}-1}\frac{E_S}{\sigma_{ij}^2}})$.

To reduce the computational complexity of (50), we can represent SI symbol power φ as a discrete RV Φ with the probability mass function $f_\Phi(\varphi)$ dependent on M_{SI}. Then, the final SEP expression as a function of γ, N_T, and the modulation orders is obtained after inserting (48) and (53) into (50)

$$P_s=\frac{1}{M_{SOI}}\sum_{n=1}^{|\Phi|}f_\Phi(\varphi_n)\Bigg(\sum_{i\in Corners}\left(2Q-Q^2\right)+\sum_{i\in Edges}\left(3Q-2Q^2\right)+\sum_{i\in Inners}\left(4Q-4Q^2\right)\Bigg), \quad (54)$$

where

$$Q=Q\left(\sqrt{\frac{3\gamma}{M_{SOI}-1}\frac{N_T}{\phi_i+\varphi_n+N_T}}\right),\ \gamma=\frac{E_S|H_{SOI}|^2}{\sigma^2}. \quad (55)$$

For M_{SOI}=4 and 16, (54) can be further simplified since each symbol category is represented by a unique power level.

$$P_s^4=\sum_{n=1}^{|\Phi|}f_\Phi(\varphi_n)\left(2Q\left(\sqrt{\frac{\gamma N_T}{1+\varphi_n+N_T}}\right)-Q^2\left(\sqrt{\frac{\gamma N_T}{1+\varphi_n+N_T}}\right)\right), \quad (56)$$

$$P_s^{16}=\sum_{n=1}^{|\Phi|}f_\Phi(\varphi_n)\Bigg(Q\left(\sqrt{\frac{0.2\gamma N_T}{0.2+\varphi_n+N_T}}\right)-Q^2\left(\sqrt{\frac{0.2\gamma N_T}{0.2+\varphi_n+N_T}}\right)+\frac{3}{2}Q\left(\sqrt{\frac{0.2\gamma N_T}{1+\varphi_n+N_T}}\right)-Q^2\left(\sqrt{\frac{0.2\gamma N_T}{1+\varphi_n+N_T}}\right)+\frac{1}{2}Q\left(\sqrt{\frac{0.2\gamma N_T}{1.8+\varphi_n+N_T}}\right)-\frac{1}{4}Q^2\left(\sqrt{\frac{0.2\gamma N_T}{1.8+\varphi_n+N_T}}\right)\Bigg), \quad (57)$$

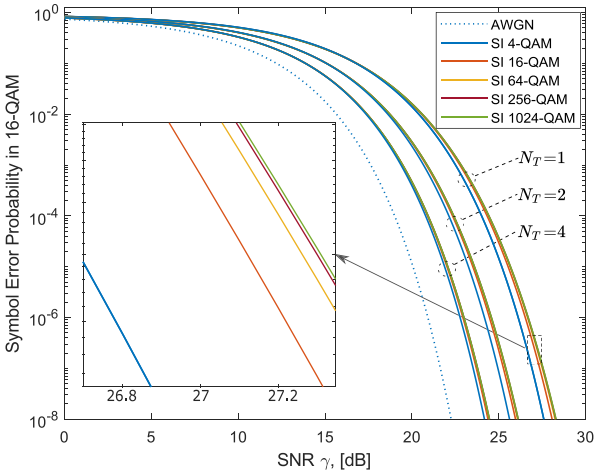

FIGURE 5. The influence of the training symbol number N_T and SI on symbol error probability in receiving 16-QAM SOI signals.

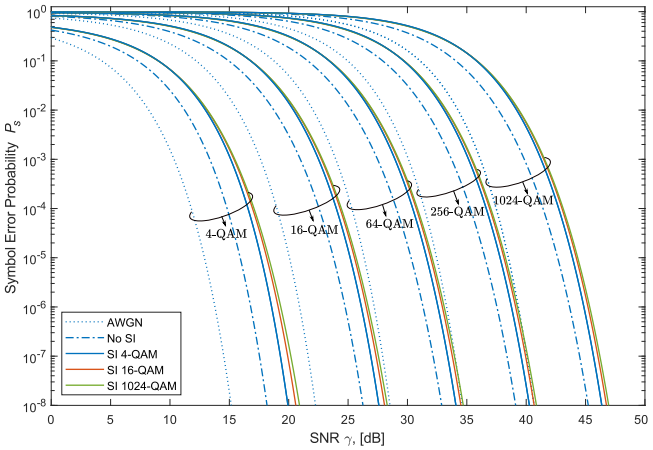

FIGURE 6. Symbol error probability in receiving M-QAM SOI signals under channel estimation errors in SISO IBFD with $N_T=1$. For each M-QAM SOI (labeled), there is a group of curves represented by the legend.

where Φ is the discrete RV representing the normalized power in an M-QAM constellation of the order M_{SI}.

The exact SEP curves given by (54) as well as (26) are plotted in Figs. 5 and 6. Fig. 5 shows the influence of N_T and M_{SI} on SEP receiving 16-QAM SOI symbols. The higher the SI modulation order, the worse the SEP for a given SNR. However, the most considerable deterioration in SEPs happens after the change of M_{SI} from 4-QAM to 16-QAM, quickly diminishing further towards 1024-QAM. Fig. 6 compares SEPs for different M-QAM in SISO IBFD with N_T=1.

D. ERROR PROBABILITY FOR M-QAM IN MIMO

The derived closed-form expressions (54)-(57) for the SEP in SISO IBFD are also applicable for SIMO IBFD and for SISO TDD and SIMO TDD if SI-related errors are set to zero. This subsection considers SEPs for MIMO communication since it has a different channel estimation procedure.

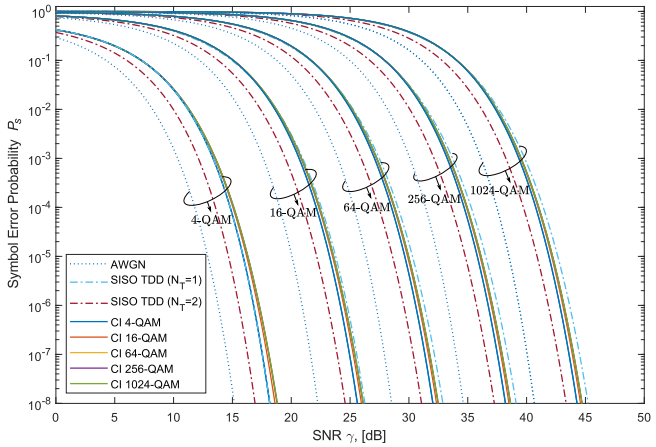

FIGURE 7. Symbol error probability in receiving M-QAM symbols under cross-interference from parallel data stream in MIMO TDD with $N_T = 2$.

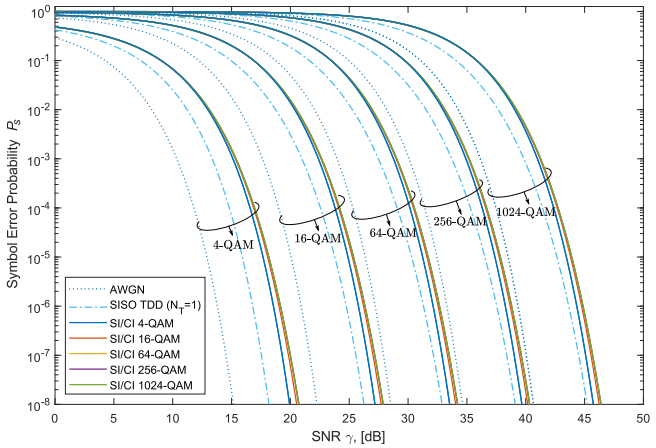

FIGURE 8. Symbol error probability in receiving M-QAM symbols under CI and SI in MIMO IBFD with $N_T = 2$.

In MIMO IBFD, four signals contribute to estimation errors. Let X_I and X_J be SOI signals and X_U and X_V be SI signals with the modulation orders M_I, M_J, M_U, and M_V respectively. The instantaneous symbol power can be expressed as $|X_I^{(i)}|^2 = E_S\,\phi_i$, $i \in \{1, M_I\}$, $|X_J^{(j)}|^2 = E_S\,\phi_j$, $j \in \{1, M_J\}$, $|X_U^{(u)}|^2 = E_S\,\varphi_u$, $i \in \{1, M_U\}$ and $|X_V^{(v)}|^2 = E_S\,\varphi_v$, $j \in \{1, M_V\}$. Then, the effective variance of ΔX_I on a constellation can be expressed in MIMO IBFD as

$$\sigma^2_{ijuv} = \mathbb{V}\Big[\Delta X_I | X_I^{(i)}, X_J^{(j)}, X_U^{(u)}, X_V^{(v)}\Big] = \left(\frac{\phi_i + \phi_j}{2(N_T-1)} + \frac{\varphi_u + \varphi_v}{2(N_T-1)} + 1\right)\sigma^2 f\left(H_{SOI}^{-1}\right), \quad (58)$$

where $f(H_{SOI}^{-1})$ is the function of channel frequency responses, similar to the expressions in Appendix D.

Similarly to (51), the probability of crossing one decision border on a constellation by receiving X_I is given by

$$P_e^I = P_e^Q = Q\left(\frac{d\sqrt{2}}{\sigma_{ijuv}}\right) = Q\left(\sqrt{\frac{3}{M_I-1}\frac{E_S}{2\,\sigma^2_{ijuv}}}\right) = Q\left(\sqrt{\frac{3\,\gamma}{M_I-1}\frac{2(N_T-1)}{2(N_T-1)+\phi_i+\varphi_n^*}}\right), \quad (59)$$

where γ is the SNR according to Table 2, ϕ_i is the normalized power of the SOI signal X_I, and $\varphi_n^* = \phi_j + \varphi_u + \varphi_v$ is a discrete RV dependent on modulation orders M_J, M_U, and M_V of the other three signals. In MIMO TDD, φ_u and φ_v equal zero; therefore, $\varphi_n^* = \phi_j$ will represent only cross-interference (CI) from parallel data steam and depends only on M_J.

In MIMO, SEPs can be computed as in (54) with redefined Q-function arguments according to (59). SEP curves are plotted for MIMO TDD in Fig. 7 and for MIMO IBFD in Fig. 8, with all three interfering signals having the same modulation order.

V. BIT ALLOCATION

The optimization problem defined in (29) must be solved for integer variables N_T and $n_{i,k}$, so it is non-convex. According to Fig. 5, the training symbol number N_T influences the effective SINR and SEP; consequently, any change of N_T affects bit allocation $n_{i,k}$ at all subcarriers. Therefore, we can replace the optimization problem (29) by two sub-problems. First, we solve (29) with respect to N_T; second, we find BA for a fixed N_T. We further provide a solution for IBFD and TDD BA in SISO, which can also be extended to the SIMO and MIMO scenarios.

A. TRAINING SYMBOL NUMBER SELECTION

To simplify the first sub-problem, the integer and discrete constraints on $n_{i,k}$ in (29) can be relaxed. Also, we can ignore the P_s term since it is irrelevant to this sub-problem. Furthermore, according to Fig. 6, the value of modulation order M_{SI} is much less important than the fact of having SI-related interference. Therefore, we can model IBFD and TDD using the SNR degradation η as defined in Table 3. Then, using (22), the optimization sub-problem is redefined for IBFD as

$$\underset{N_T>0}{\text{maximize}} \left(1 - \frac{2N_T}{N_{CT}}\right) \sum_{i=1}^{N_{TX}} \sum_{k=1}^{N_{asc}} \log_2\left(1 + \frac{\gamma_{i,k}}{\Gamma}\frac{N_T}{N_T+2}\right). \quad (60)$$

Since 4-QAM is the lowest modulation order we consider, we can add a constraint to (60)

$$\log_2\left(1 + \frac{\gamma_{i,k}}{\Gamma}\frac{N_T}{N_T+2}\right) \geq 2 \forall i, k, N_T. \quad (61)$$

According to [13], IBFD is the most beneficial for the subcarriers with high SNR. Hence, the optimal N_T in IBFD should be influenced mainly by high SNR frequencies. With respect to high SNR subcarriers, we can simplify the constraint in (61) as $\gamma_{i,k} \geq 9\Gamma$ and replace $\log_2(1+\frac{\gamma_{i,k}}{\Gamma}\frac{N_T}{N_T+2})$ in (60) with $\log_2(\frac{\gamma_{i,k}}{\Gamma}\frac{N_T}{N_T+2})$. The optimization sub-problem has a global solution in small integer values of N_T [13]. Thus,

Algorithm 1 Selecting Training Symbol Number in IBFD

Input: $\{\gamma_{i,k}\}$, N_{TX}, N_{asc}, N_{CT}

$K \leftarrow 0$, $\gamma_\Sigma \leftarrow 0$
for $i = 1 : N_{TX}$, $k = 1 : N_{asc}$ **do**
  if $\gamma_{i,k} \geq 9\Gamma$ **then**
    $\gamma_\Sigma \leftarrow \gamma_\Sigma + 10\log_{10}(\gamma_{i,k})$, $K \leftarrow K + 1$
  end if
end for
$n \leftarrow 1$, $N \leftarrow N_{CT}$, $\bar{\gamma}_{dB} \leftarrow \gamma_\Sigma/K - 10\log_{10}\Gamma$
while $5(N-2n)\log_{10}\frac{(n+1)(n+2)}{n(n+3)} + 10\log_{10}\frac{n+3}{n+1} > \bar{\gamma}_{dB}$ **do** $n \leftarrow n+1$
end while
return n

the optimal N_T can be found by an iterative subroutine that consequently checks the objective function until it reaches the maximum. Let J_n be a cost function at the n-th iteration defined $\forall n \in \{1, \ldots, \frac{N}{2}\}$ and $\forall k \in \{1, \ldots, K \leq N_{TX} \times N_{asc}\}$ as

$$J_n = \left(1 - \frac{2n}{N}\right) \sum_{k=1}^{K} \log_2\left(\frac{\gamma_k}{\Gamma}\frac{n}{n+2}\right). \tag{62}$$

Starting with $n = 1$, we increment n if $J_{n+1} > J_n$ is satisfied. The optimal solution is the first n for which the condition is no longer satisfied. The condition $J_{n+1} > J_n$ can be rewritten as follows

$$\begin{aligned}
&\left(1 - \frac{2n+2}{N}\right) \sum_{k=1}^{K} \log_2 \frac{\gamma_k}{\Gamma}\frac{n+1}{n+3} > \left(1 - \frac{2n}{N}\right) \sum_{k=1}^{K} \log_2 \frac{\gamma_k}{\Gamma}\frac{n}{n+2},\\
&\frac{N-2n-2}{N} K \log_2 \frac{n+1}{n+3} - \frac{N-2n}{N} K \log_2 \frac{n}{n+2} > \frac{2}{N} \sum_{k=1}^{K} \log_2 \frac{\gamma_k}{\Gamma},\\
&(N-2n-2)\log_2 \frac{n+1}{n+3} + (N-2n)\log_2 \frac{n+2}{n} > \frac{2}{K} \sum_{k=1}^{K} \log_2 \frac{\gamma_k}{\Gamma},\\
&5(N-2n)\log_{10} \frac{(n+1)(n+2)}{n(n+3)} + 10\log_{10} \frac{n+3}{n+1} > \frac{10}{K} \sum_{k=1}^{K} \log_{10} \frac{\gamma_k}{\Gamma}.
\end{aligned} \tag{63}$$

From (63), the optimal training symbol N_T^{opt} can be determined based on the total number of OFDM symbols N_{CT} and the average SNR in dB. The higher the average SNR in dB, the fewer training symbols are needed. Algorithm 1 shows the pseudo-code to compute the optimal training symbol number N_T^{opt}. Algorithm 1 can also be applied in TDD by correcting η and ρ based on (24) and Table 3. The check condition in TDD is

$$10(N-n)\log_{10}\frac{(n+1)(n+1)}{n(n+2)} + 10\log_{10}\frac{n+2}{n+1} > \bar{\gamma}_{dB}, \tag{64}$$

where $\bar{\gamma}_{dB}$ is the average SNR in dB corrected for Γ computed over all subcarriers with the SNR higher than 6Γ.

B. COOPERATIVE BIT ALLOCATION

The second optimization sub-problem can be reformulated for each subcarrier independently. Let $P_s(\gamma, n_{SOI}, n_{SI}, N_T)$ be the SEP function defined in (54). Then, in SISO IBFD, for signals with the SNR γ_i and γ_j, bit allocations n_i and n_j can be determined as follows

$$\begin{aligned}
\underset{n_i,n_j}{\text{maximize}}\ & n_i + n_j - P_s\big(\gamma_i, n_i, n_j, N_T\big) - P_s\big(\gamma_j, n_j, n_i, N_T\big)\\
\text{subject to}\ & n_i, n_j \in \{0, 2, 4, 6, 8, 10\},\\
& P_s\big(\gamma_i, n_i, n_j, N_T\big) \leq P_0,\\
& P_s\big(\gamma_j, n_j, n_i, N_T\big) \leq P_0.
\end{aligned} \tag{65}$$

If n_i^0 and n_j^0 are bit loading without interference (or in TDD) at subcarriers with SNRs γ_i and γ_j so that $P_s(\gamma_i, n_i^0, 0, N_T) \leq P_0$ and $P_s(\gamma_j, n_j^0, 0, N_T) \leq P_0$, we need to consider only four pairs as candidates for the optimal solution in IBFD: (n_i^0, n_j^0), $(n_i^0, n_j^0 - 2)$, $(n_i^0 - 2, n_j^0)$, and $(n_i^0 - 2, n_j^0 - 2)$.

Let $\mathcal{C}(n_i, n_j)$ be a function that checks both SEP constraints $P_s(\gamma_i, n_i, n_j, N_T) \leq P_0$ and $P_s(\gamma_j, n_j, n_i, N_T) \leq P_0$ in (65). Then, the pair (n_i^0, n_j^0) will be the optimal solution if $\mathcal{C}(n_i^0, n_j^0)$ returns true. Otherwise, the search will continue for the next pairs. If both pairs $(n_i^0, n_j^0 - 2)$ and $(n_i^0 - 2, n_j^0)$ satisfy the constraints, a cooperative decision between nodes is required. From the pairs $(n_i^0, n_j^0 - 2)$ and $(n_i^0 - 2, n_j^0)$, a pair that minimizes the sum of symbol error probabilities in (65) is the optimal solution. From Fig. 6, the pair $(n_i^0 - 2, n_j^0 - 2)$ will always satisfy the constraints since if $P_s(\gamma_i, n_i^0, 0, N_T) \leq P_0$, then $P_s(\gamma_i, n_i^0 - 2, n_j, N_T) \leq P_0$ is also satisfied $\forall n_j$.

The values n_i^0 and n_j^0 can be estimated using the SNR gap approach

$$n_i^0 \leq \log_2\left(1 + \frac{\gamma_i}{\Gamma}\frac{N_T}{N_T + 1}\right), \tag{66}$$

where Γ is the SNR gap defined in (23).

C. BIT ALLOCATION ALGORITHM

We assume that the nodes start communication using 4-QAM and any reasonable but fixed N_T. The nodes perform error vector magnitude (EVM) measurements on a constellation diagram, which can later be used for the SNR estimation and obtaining BA to increase throughput. The root-mean-square (RMS) EVM can be computed at the k-th subcarrier over multiple OFDM symbols as follows

$$EVM_k = \frac{\sqrt{\frac{1}{L}\sum_{l=1}^{L} |\hat{S}_{l,k} - S_{l,k}|^2}}{\sqrt{\frac{1}{L}\sum_{l=1}^{L} |S_{l,k}|^2}}, \tag{67}$$

where L is the number of OFDM symbols considered, $S_{l,k}$ and $\hat{S}_{l,k}$ are the transmitted and the received constellation points on the k-th subcarrier at the l-th OFDM symbol.

Since the RMS EVM evaluates the sample variance of ΔX_{SOI}, which asymptotically converges to (46), sufficient statistics is achieved when $L \gg N_P$. The nodes can estimate SNR γ at each subcarrier by correcting SINR with the actual

SNR degradation η based on Table 3. For SISO IBFD, SNR γ_k is estimated based on the EVM measurements as

$$\hat{\gamma}_k = \frac{1}{EVM_k^2}\frac{1}{\eta} = \frac{1}{EVM_k^2}\left(\frac{2}{N_T}+1\right). \tag{68}$$

Once information about γ_k is available and exchanged between nodes, nodes can compute the optimal training symbol number N_T^{opt} and bit loading for all transmitters and subcarriers. The nodes can perform BA to maximize the bidirectional throughput (cooperative allocation) as well as to maximize throughput in one direction while keeping predefined rates in another direction. Unidirectional throughput optimization can be useful in two situations: 1) in the beginning, when all γ_k are not available, but one of the nodes has already collected sufficient statistics, and 2) a node has a small amount of data to transmit, and 4-QAM is sufficient and preferable. Algorithm 2 presents the procedure for adaptive BA, including bidirectional and unidirectional throughput optimization in SISO IBFD. Furthermore, the nodes can negotiate switching to any other communication scenario. Knowing all required channel frequency responses, the nodes can recompute SNRs, the expected SNR degradation, and BA for another communication mode using Tables 2 and 3.

Algorithm 2 Adaptive Bit Allocation in SISO IBFD

Input: N_T, N_{asc}, P_0, ▷ Independently on each node
$\{n_{p,k}\} \leftarrow \{2\}$, $\{n_{q,k}\} \leftarrow \{2\}$ $\forall p \in SOI, \forall q \in SI$
for $k = 1{:}N_{asc}$, $\forall p \in SOI$ **do**
  Measure and estimate $EVM_{p,k}$ using (67)
  Compute $\gamma_{p,k}$ using (68) and Table 3
  $n_{p,k} \leftarrow$ BITALLOC($\gamma_{p,k}$, $n_{q,k}$, N_T, P_0)
end for
Send $\{n_{p,k}\}$ **or** $\{\gamma_{p,k}\}$ to the opposite node $\forall p \in SOI$
function COOPBITALLOC(γ_i, γ_j, N_T, P_0)
  Compute n_i^0 and n_j^0 using (66)
  $n_i \leftarrow n_i^0$, $n_j \leftarrow n_j^0$
  while $\sim \mathcal{C}(n_i, n_j)$ **do**
    $S_i \leftarrow P_s(\gamma_i, n_i-2, n_j, N_T) + P_s(\gamma_j, n_j, n_i-2, N_T)$
    $S_j \leftarrow P_s(\gamma_i, n_i, n_j-2, N_T) + P_s(\gamma_j, n_j-2, n_i, N_T)$
    if $S_i < S_j$ **then** $n_i \leftarrow n_i - 2$
    end if
    if $S_j < S_i$ **then** $n_j \leftarrow n_j - 2$
    end if
  end while
  return (n_i, n_j)
end function
function BITALLOC(γ, n_{SI}, N_T, P_0)
  Compute n_p^0 using (66) $\forall p \in SOI$
  if $\mathcal{C}(n_p^0, n_{SI})$ **then return** (n_p^0, n_{SI})
  else return $(n_p^0 - 2, n_{SI})$
  end if
end function
procedure ONRECEIVE($\{\gamma_k\}$ **or** $\{n_k\}$ **or** N_T^{opt})
  Update $\{\gamma_{q,k}\} \leftarrow \{\gamma_k\}$ **or** $\{n_{q,k}\} \leftarrow \{n_k\}$ **or** $N_T \leftarrow N_T^{opt}$
  Update N_T if $\gamma_{p,k}$, $\gamma_{q,k}$ available using Algorithm 1
  Update $\{n_{p,k}\}$ if any changes in $\{n_{q,k}\}$ or N_T
  $(n_{p,k}, n_{q,k}) \leftarrow$ COOPBITALLOC($\gamma_{p,k}$, $\gamma_{q,k}$, N_T, P_0)
  Send all updates to the opposite node
end procedure

VI. NUMERICAL RESULTS

In this section, we evaluate the proposed BA and the overall IBFD performance over measured 2x2 MIMO channels [13, Fig. 3]. We compare IBFD and TDD communication in the SISO, SIMO, and MIMO scenarios in two frequency bands.

A. SYSTEM CONFIGURATION

We use OFDM system parameters from the G.hn standard [17], [24]. All nodes generate OFDM baseband signals in the frequency range up to 100 MHz with the subcarrier spacing of f_{sc}=24.4140625 kHz. All OFDM symbols have a duration of T_S=51.2 μs, the total number of subcarriers (the FFT size) of up to N_{fft}=4096, and the cyclic prefix of N_{cp}=N_{fft}/4 samples without pulse shaping. The transmission frame is assumed to be limited by approximately 1-2 ms [11], due to the LPTV nature of the BB-PLC medium, corresponding to 20-40 OFDM symbols in total.

The PSD of a transmitted signal is limited by −55 dBm/Hz in 2-30 MHz and by −85 dBm/Hz in 30-100 MHz. The noise model is a background noise with the frequency-dependent PSD (18) in the worst-case scenario, as shown in Fig. 3. The subcarriers 0-73 (0-1.8 MHz) are masked. The notches in the Amateur Radio Bands are in force, affecting the subcarriers in the bands 1.8-2.0 MHz, 3.5-4.0 MHz, 7.0-7.3 MHz, 10.1-10.15 MHz, 14.0-14.35 MHz, 18.068-18.168 MHz, 21.0-21.45 MHz, 24.89-24.99 MHz, 28.0-29.7 MHz, 50.0-54.0 MHz, and 69.9-70.5 MHz. The maximum number of active subcarriers is N_{asc}=3662 with 985 and 2677 subcarriers in 2-30 MHz and 30-100 MHz, correspondingly.

B. EVALUATION OF BIT ALLOCATION ALGORITHM

We evaluate the proposed BA algorithm in 2-30 MHz for SISO and SIMO with the LN and RN utilizing TX1 and TX2 for transmission and MIMO with all four transmitters.

To evaluate the subroutine in Algorithm 1, we compare the throughput for different N_T with the throughput for N_T^{opt} returned by Algorithm 1. For the channel shown in Fig. 9, the subroutine provided a near-optimal training symbol number for the transmitter TX2 in SISO TDD, resulting in not achieving the highest possible throughput, as illustrated in Fig. 10. To understand how often such a situation occurs, we introduce the throughput loss metric and characterize it over the channel database for different communication modes. The throughput loss in percent is defined as

$$\Delta T = \frac{T - \hat{T}}{T} \times 100\%, \tag{69}$$

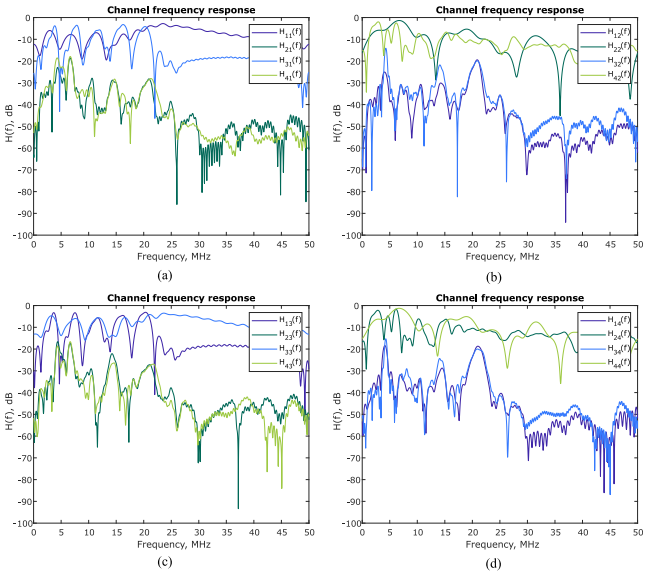

FIGURE 9. An example of 2x2 MIMO channel. Channels are seen at (a) RX1, (b) RX2, (c) RX3, and (d) RX4.

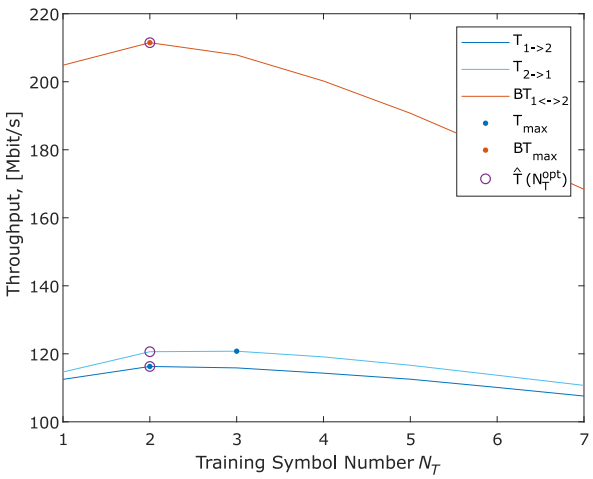

FIGURE 10. Throughput versus the training symbol number in SISO communication with $N_{CT} = 40$ for the channel example in Fig. 9.

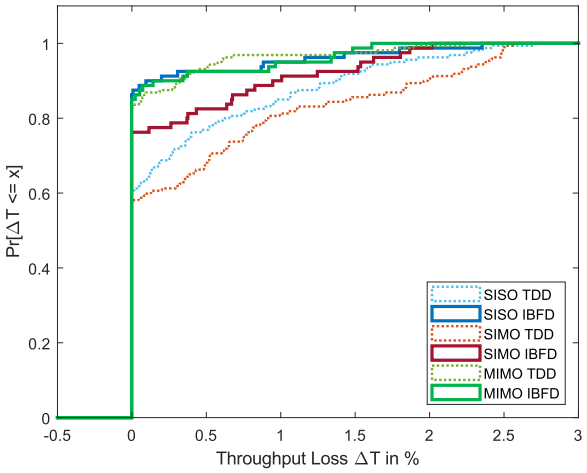

FIGURE 11. The CDF of throughput loss in % in the considered communication modes by using the proposed training symbol number selection subroutine with $N_{CT} = 40$.

TABLE 4. Percentage of cases in which a given N_T is optimal by IBFD and TDD in SISO, SIMO, and MIMO with $N_{CT} = 20$ and $N_{CT} = 40$.

	$N_{CT}=20$				$N_{CT}=40$			
N_T	1	2	3	4	1	2	3	4
SISO TDD	50.6	49.4	0	0	20.6	50.6	28.1	0
SISO IBFD	90	10	0	0	26.3	71.2	2.5	0
SIMO TDD	71.9	28.1	0	0	35.6	57.5	6.9	0
SIMO IBFD	100	0	0	0	48.8	50	1.2	0
MIMO TDD	n/a	51.2	48.8	0	n/a	8.8	60.6	30.6
MIMO IBFD	n/a	91.2	8.80	0	n/a	15	80	5

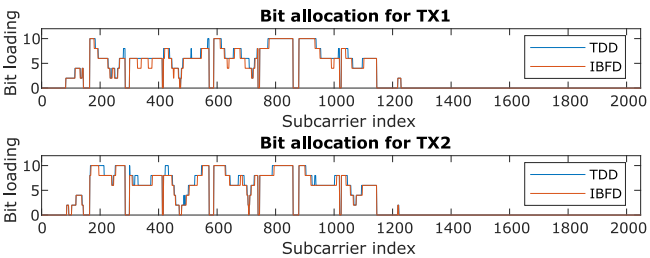

FIGURE 12. Bit allocation example in SISO TDD and IBFD communication.

where T is the maximum throughput determined by the exhaustive search over N_T, and $\hat{T}$ is the throughput computed for N_T^{opt} provided by Algorithm 1.

Fig. 11 shows the cumulative distribution function (CDF) of the throughput loss for $N_{CT} = 40$. Overall, the proposed subroutine returns an optimal N_T in more than 76% of cases for IBFD, 56% of cases for TDD (both worst in SIMO), and the highest registered throughput loss is 2.71%, which is an acceptable result. For lower N_{CT}, Algorithm 1 performs better; throughput loss occurs less frequently, but its maximum value may slightly increase. Information about how often a given N_T is optimal by different communication scenarios and two values of N_{CT} is provided in Table 4.

An example of bit allocation in SISO is shown in Fig. 12, where a decrease in transmission rate can be observed in IBFD for some subcarriers. Fig. 13 illustrates the SEP for IBFD and TDD at all subcarriers of both nodes with the SEP threshold $P_0 = 10^{-2}$ in SISO, SIMO, and MIMO. Additional interference in IBFD may cause not only lowering the modulation order but also switching off transmission for one of the streams at specific subcarriers, as depicted in Fig. 13.

Fig. 14a shows an increase in throughput for transmitters by increasing the SEP threshold P_0 (relaxing requirements) in all communication modes. Also, the IBFD throughput gain (see Fig. 14b) can be characterized as having a slight gradual increase toward higher P_0,

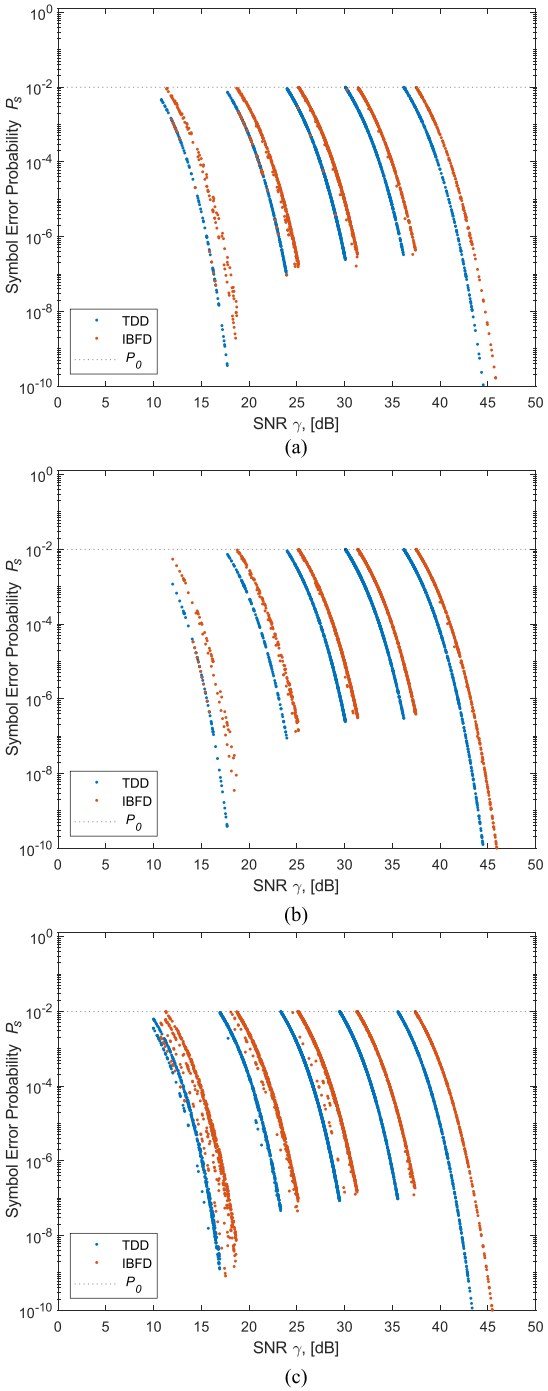

FIGURE 13. Symbol error probability in IBFD and TDD communication for (a) SISO, (b) SIMO, and (c) MIMO. The SNR values correspond to the subcarriers in 2-30 MHz for the channel realization in Fig. 9.

confirming IBFD to be more beneficial under low SEP requirements.

C. ACHIEVABLE THROUGHPUT IN TWO FREQUENCY BANDS

Due to the transmission power limitation in 30-100 MHz, which is 30 dB lower compared to 2-30 MHz, the 30-100 MHz range is expected to have much lower SNRs

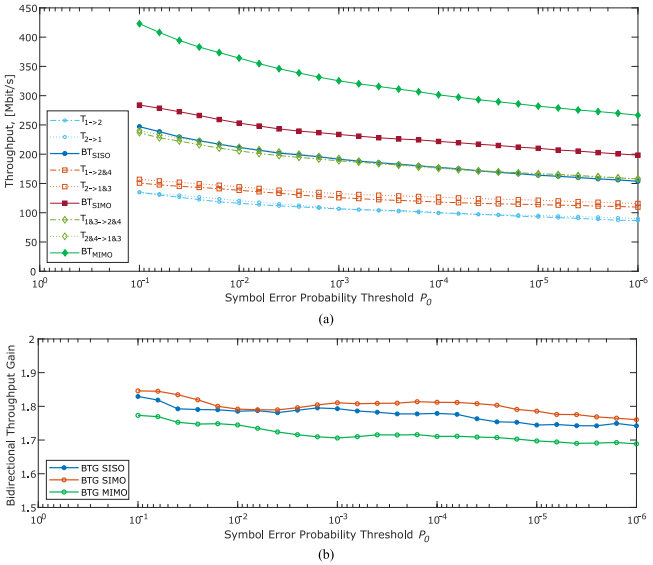

FIGURE 14. The influence of P_0 on (a) throughput and (b) BTG in SISO, SIMO, and MIMO communication. TDD is represented by throughput T for each node, IBFD is represented by bidirectional throughput BT of the two nodes.

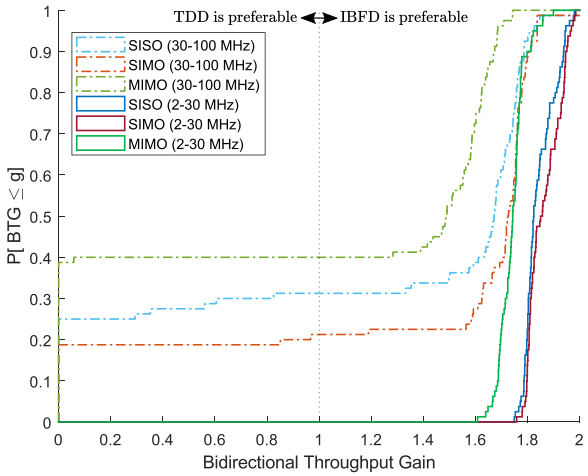

FIGURE 15. The CDF of the BTG offered by IBFD in SISO, SIMO and MIMO in 2-30 MHz and 30-100 MHz.

at the receiver side and, consequently, offers lower rates per subcarrier. We analyze the IBFD performance separately for the two frequency bands. Bidirectional throughput and bidirectional throughput gain (BTG) are computed in all communication scenarios at their near-optimal N_T^{opt} with N_{CT}=40 and P_0=10^{-2}. For SISO and SIMO, we compute the bidirectional throughput for the best link options between the nodes.

Fig. 15 depicts the BTG results for the database of measured 2x2 MIMO channels. In 2-30 MHz, BTGs vary from 1.61 to 1.98, with the median values of 1.82, 1.85, and 1.74 for SISO, SIMO, and MIMO correspondingly. In 30-100 MHz, many channels are unusable, causing the median IBFD BTGs to drop to 1.67, 1.72, and 1.49. The expected bidirectional throughput in IBFD and TDD BB-PLC in the two frequency ranges is presented in Fig. 16. In 2-30 MHz,

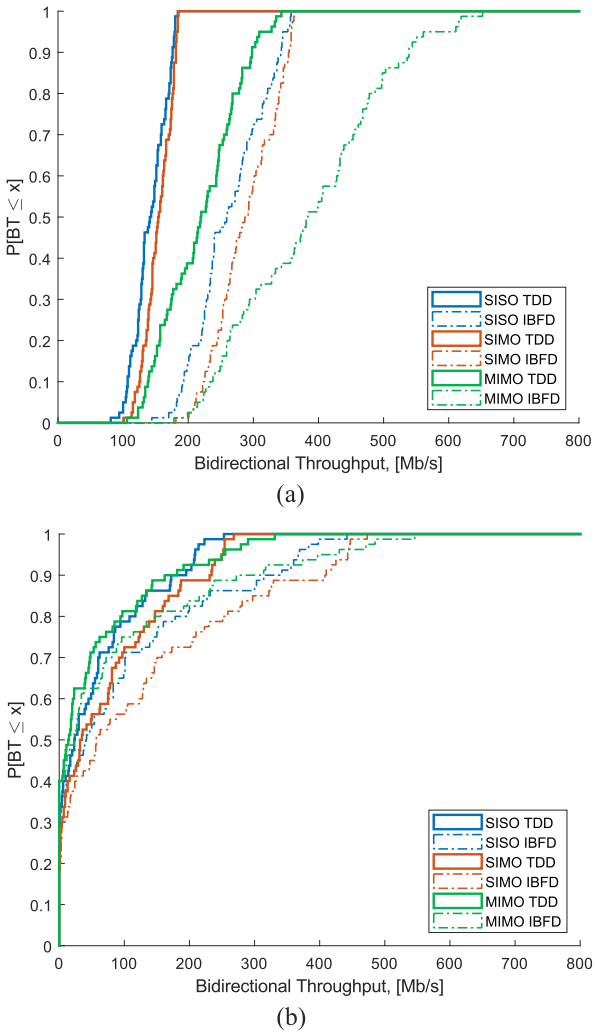

FIGURE 16. The CDF of the bidirectional throughput in SISO, SIMO and MIMO BB-PLC in (a) 2-30 MHz and (b) 30-100 MHz.

the median IBFD bidirectional throughput reaches 260 Mb/s in SISO, 290 Mb/s in SIMO, and 383 Mb/s in MIMO. In 30-100 MHz, the median IBFD bidirectional throughput reaches only 43 Mb/s in SISO, 57 Mb/s in SIMO, and 23 Mb/s in MIMO.

VII. CONCLUSION

This paper considered IBFD and TDD BB-PLC communication under imperfect channel estimation in SISO, SIMO, and MIMO scenarios. Section IV showed the effect of SI and its applied modulation order on symbol error probability. The influence of SI modulation order can be explained by higher instantaneous SINR variations compared to the average SINR in higher M-QAM. The effect is more prominent at high SNR frequencies and can be diminished by utilizing more training OFDM symbols (Fig. 5). In Section V, a bit allocation algorithm was proposed that considers such symbol error probability degradation. The algorithm also includes a subroutine for selecting the training symbol number to maximize the bidirectional throughput in BB-PLC.

The practical importance of this work is threefold. First, the derived symbol error probability expressions help to better understand the opportunities (achievable throughput) of IBFD in BB-PLC. IBFD is especially attractive in 2-30 MHz, where the throughput can be improved by 82%, 85%, and 74% in SISO, SIMO, and MIMO, respectively. Second, the paper targeted the problem of assigning a number of symbols for channel estimation. The proposed Algorithm 1 helps to select a proper number of training OFDM symbols to achieve the best spectral efficiency using the IBFD technology. Third, this paper thoroughly analyzed IBFD in communication scenarios such as SISO, SIMO, and MIMO. The work estimated the expected SINR and symbol error probabilities in the considered scenarios, allowing recalculation of bit allocation for another communication mode without redoing EVM measurements. This can be useful when an opportunistic transition to IBFD is considered after obtaining channel state information in TDD. Moreover, the proposed Algorithm 2 can adapt the bit allocation in IBFD to maximize throughput in one or both directions.

APPENDIX

A. ERROR VECTORS IN SIMO IBFD

Let's consider SIMO communication, where the LN transmits data by the transmitter TX1, the RN sends data by the transmitter TX2, and both nodes decode data using all available receivers. The signals in (4) for the LN and in (7) for the RN can be rewritten as

$$\begin{bmatrix} Y_{AIC1} \\ Y_{AIC3} \end{bmatrix} = \begin{bmatrix} \Delta H_{11} \\ \Delta H_{13} \end{bmatrix} X_1 + \begin{bmatrix} H_{21} \\ H_{23} \end{bmatrix} X_2 + \begin{bmatrix} W_1 \\ W_3 \end{bmatrix}, \tag{70}$$

$$\begin{bmatrix} Y_{AIC2} \\ Y_{AIC4} \end{bmatrix} = \begin{bmatrix} H_{12} \\ H_{14} \end{bmatrix} X_1 + \begin{bmatrix} \Delta H_{22} \\ \Delta H_{24} \end{bmatrix} X_2 + \begin{bmatrix} W_2 \\ W_4 \end{bmatrix}. \tag{71}$$

Using Maximum Ratio Combining (MRC), we can obtain data at the LN

$$\hat{X}_2 = \frac{Y_{AIC1}\hat{H}_{21}^* + Y_{AIC3}\hat{H}_{23}^*}{\left|\hat{H}_{21}\right|^2 + \left|\hat{H}_{23}\right|^2}. \tag{72}$$

After simplifications, we obtain

$$\begin{aligned} \hat{X}_2 = X_2 &+ \frac{\Delta H_{11}\hat{H}_{21}^* + \Delta H_{13}\hat{H}_{23}^*}{\left|\hat{H}_{21}\right|^2 + \left|\hat{H}_{23}\right|^2} X_1 \\ &+ \frac{\Delta H_{21}\hat{H}_{21}^* + \Delta H_{23}\hat{H}_{23}^*}{\left|\hat{H}_{21}\right|^2 + \left|\hat{H}_{23}\right|^2} X_2 + \frac{W_1\hat{H}_{21}^* + W_3\hat{H}_{23}^*}{\left|\hat{H}_{21}\right|^2 + \left|\hat{H}_{23}\right|^2}. \end{aligned} \tag{73}$$

Error in data at the LN receivers is given by

$$\begin{aligned} \Delta X_2 = &\frac{\Delta H_{11}\hat{H}_{21}^* + \Delta H_{13}\hat{H}_{23}^*}{\left|\hat{H}_{21}\right|^2 + \left|\hat{H}_{23}\right|^2} X_1 \\ &+ \frac{\Delta H_{21}\hat{H}_{21}^* + \Delta H_{23}\hat{H}_{23}^*}{\left|\hat{H}_{21}\right|^2 + \left|\hat{H}_{23}\right|^2} X_2 + \frac{W_1\hat{H}_{21}^* + W_3\hat{H}_{23}^*}{\left|\hat{H}_{21}\right|^2 + \left|\hat{H}_{23}\right|^2}. \end{aligned} \tag{74}$$

Similarly, error in data at the RN receivers is given by

$$\Delta X_1 = \frac{\Delta H_{22}\hat{H}_{12}^* + \Delta H_{24}\hat{H}_{14}^*}{\left|\hat{H}_{12}\right|^2 + \left|\hat{H}_{14}\right|^2} X_2$$

$$+\frac{\Delta H_{12}\hat{H}_{12}^{*}+\Delta H_{14}\hat{H}_{14}^{*}}{\left|\hat{H}_{12}\right|^{2}+\left|\hat{H}_{14}\right|^{2}}X_1+\frac{W_2\hat{H}_{12}^{*}+W_4\hat{H}_{14}^{*}}{\left|\hat{H}_{12}\right|^{2}+\left|\hat{H}_{14}\right|^{2}}. \tag{75}$$

The expressions (74) and (75) can be decomposed into three error components, as in (36).

B. ERROR VECTORS IN MIMO IBFD

From (4) and (7), the data at the LN and the RN receivers can be decoded as

$$\begin{bmatrix}\hat{X}_2\\ \hat{X}_4\end{bmatrix}=\begin{bmatrix}\hat{H}_{21} & \hat{H}_{41}\\ \hat{H}_{23} & \hat{H}_{43}\end{bmatrix}^{-1}\cdot\begin{bmatrix}Y_{AIC1}\\ Y_{AIC3}\end{bmatrix}, \tag{76}$$

$$\begin{bmatrix}\hat{X}_1\\ \hat{X}_3\end{bmatrix}=\begin{bmatrix}\hat{H}_{12} & \hat{H}_{32}\\ \hat{H}_{14} & \hat{H}_{34}\end{bmatrix}^{-1}\cdot\begin{bmatrix}Y_{AIC2}\\ Y_{AIC4}\end{bmatrix}. \tag{77}$$

Following the same approach as in SISO and SIMO, we obtained expressions for the data errors in MIMO IBFD. The error vectors on a constellation are given by

$$\begin{bmatrix}\Delta X_2\\ \Delta X_4\end{bmatrix}=\begin{bmatrix}\hat{H}_{21} & \hat{H}_{41}\\ \hat{H}_{23} & \hat{H}_{43}\end{bmatrix}^{-1}\cdot\left(\begin{bmatrix}\Delta H_{11} & \Delta H_{31}\\ \Delta H_{13} & \Delta H_{33}\end{bmatrix}\begin{bmatrix}X_1\\ X_3\end{bmatrix}+\begin{bmatrix}\Delta H_{21} & \Delta H_{41}\\ \Delta H_{23} & \Delta H_{43}\end{bmatrix}\begin{bmatrix}X_2\\ X_4\end{bmatrix}+\begin{bmatrix}W_1\\ W_3\end{bmatrix}\right). \tag{78}$$

$$\begin{bmatrix}\Delta X_1\\ \Delta X_3\end{bmatrix}=\begin{bmatrix}\hat{H}_{12} & \hat{H}_{32}\\ \hat{H}_{14} & \hat{H}_{34}\end{bmatrix}^{-1}\cdot\left(\begin{bmatrix}\Delta H_{12} & \Delta H_{32}\\ \Delta H_{14} & \Delta H_{34}\end{bmatrix}\begin{bmatrix}X_1\\ X_3\end{bmatrix}+\begin{bmatrix}\Delta H_{22} & \Delta H_{42}\\ \Delta H_{24} & \Delta H_{44}\end{bmatrix}\begin{bmatrix}X_2\\ X_4\end{bmatrix}+\begin{bmatrix}W_2\\ W_4\end{bmatrix}\right). \tag{79}$$

Performing some manipulations, we obtain the closed-form expressions for the error vectors ΔX_2 and ΔX_4 at the LN

$$\begin{bmatrix}\Delta X_2\\ \Delta X_4\end{bmatrix}=\frac{1}{\hat{H}_{43}\hat{H}_{21}-\hat{H}_{23}\hat{H}_{41}}\begin{bmatrix}\hat{H}_{43} & -\hat{H}_{41}\\ -\hat{H}_{23} & \hat{H}_{21}\end{bmatrix}\cdot\begin{bmatrix}\Delta H_{11}X_1+\Delta H_{31}X_3+\Delta H_{21}X_2+\Delta H_{41}X_4+W_1\\ \Delta H_{13}X_1+\Delta H_{33}X_3+\Delta H_{23}X_2+\Delta H_{43}X_4+W_3\end{bmatrix}, \tag{80}$$

$$\begin{aligned}\Delta X_2=&\frac{\left(\hat{H}_{43}\Delta H_{11}-\hat{H}_{41}\Delta H_{13}\right)X_1+\left(\hat{H}_{43}\Delta H_{31}-\hat{H}_{41}\Delta H_{33}\right)X_3}{\hat{H}_{43}\hat{H}_{21}-\hat{H}_{23}\hat{H}_{41}}\\&+\frac{\left(\hat{H}_{43}\Delta H_{21}-\hat{H}_{41}\Delta H_{23}\right)X_2+\left(\hat{H}_{43}\Delta H_{41}-\hat{H}_{41}\Delta H_{43}\right)X_4}{\hat{H}_{43}\hat{H}_{21}-\hat{H}_{23}\hat{H}_{41}}\\&+\frac{\hat{H}_{43}W_1-\hat{H}_{41}W_3}{\hat{H}_{43}\hat{H}_{21}-\hat{H}_{23}\hat{H}_{41}},\end{aligned} \tag{81}$$

$$\begin{aligned}\Delta X_4=&\frac{\left(\hat{H}_{21}\Delta H_{13}-\hat{H}_{23}\Delta H_{11}\right)X_1+\left(\hat{H}_{21}\Delta H_{33}-\hat{H}_{23}\Delta H_{31}\right)X_3}{\hat{H}_{43}\hat{H}_{21}-\hat{H}_{23}\hat{H}_{41}}\\&+\frac{\left(\hat{H}_{21}\Delta H_{23}-\hat{H}_{23}\Delta H_{21}\right)X_2+\left(\hat{H}_{21}\Delta H_{43}-\hat{H}_{23}\Delta H_{41}\right)X_4}{\hat{H}_{43}\hat{H}_{21}-\hat{H}_{23}\hat{H}_{41}}\\&+\frac{\hat{H}_{21}W_1-\hat{H}_{23}W_3}{\hat{H}_{43}\hat{H}_{21}-\hat{H}_{23}\hat{H}_{41}}.\end{aligned} \tag{82}$$

From (78)-(82), we can generalize that any error vector ΔX in MIMO can also be represented as the sum of three components defined in (36).

C. ERROR VECTOR VARIANCE IN SIMO IBFD

The variance of ΔX_2 in (74) for SIMO IBFD can be computed under the simplification that $\hat{H}_{ij}\approx H_{ij}$. The

$$\begin{aligned}\mathbb{V}[E_{SI}]=\mathbb{E}\left[|E_{SI}|^2\right]=&\mathbb{E}\left[\left(\frac{\left(\hat{H}_{43}\Delta H_{11}-\hat{H}_{41}\Delta H_{13}\right)X_1}{\hat{H}_{43}\hat{H}_{21}-\hat{H}_{23}\hat{H}_{41}}\right)\left(\frac{\left(\hat{H}_{43}\Delta H_{11}-\hat{H}_{41}\Delta H_{13}\right)X_1}{\hat{H}_{43}\hat{H}_{21}-\hat{H}_{23}\hat{H}_{41}}\right)^{*}\right]\\&+\mathbb{E}\left[\left(\frac{\left(\hat{H}_{43}\Delta H_{31}-\hat{H}_{41}\Delta H_{33}\right)X_3}{\hat{H}_{43}\hat{H}_{21}-\hat{H}_{23}\hat{H}_{41}}\right)\left(\frac{\left(\hat{H}_{43}\Delta H_{31}-\hat{H}_{41}\Delta H_{33}\right)X_3}{\hat{H}_{43}\hat{H}_{21}-\hat{H}_{23}\hat{H}_{41}}\right)^{*}\right]\\=&\frac{\mathbb{E}\left[|X_1|^2\right]\left(|H_{43}|^2\mathbb{E}\left[|\Delta H_{11}|^2\right]+|H_{41}|^2\mathbb{E}\left[|\Delta H_{13}|^2\right]\right)}{|H_{43}H_{21}-H_{23}H_{41}|^2}+\frac{\mathbb{E}\left[|X_3|^2\right]\left(|H_{43}|^2\mathbb{E}\left[|\Delta H_{31}|^2\right]+|H_{41}|^2\mathbb{E}\left[|\Delta H_{33}|^2\right]\right)}{|H_{43}H_{21}-H_{23}H_{41}|^2}\\=&\frac{\frac{E_S}{2}\left(\frac{|H_{43}|^2\sigma^2}{(N_T-1)E_S}+\frac{|H_{41}|^2\sigma^2}{(N_T-1)E_S}\right)}{|H_{43}H_{21}-H_{23}H_{41}|^2}+\frac{\frac{E_S}{2}\left(\frac{|H_{43}|^2\sigma^2}{(N_T-1)E_S}+\frac{|H_{41}|^2\sigma^2}{(N_T-1)E_S}\right)}{|H_{43}H_{21}-H_{23}H_{41}|^2}=\frac{\sigma^2}{(N_T-1)}\frac{|H_{43}|^2+|H_{41}|^2}{|H_{43}H_{21}-H_{23}H_{41}|^2}.\end{aligned} \tag{92}$$

$$\begin{aligned}\mathbb{V}[E_{SOI}]=\mathbb{E}\left[|E_{SOI}|^2\right]=&\mathbb{E}\left[\left(\frac{\left(\hat{H}_{43}\Delta H_{21}-\hat{H}_{41}\Delta H_{23}\right)X_2}{\hat{H}_{43}\hat{H}_{21}-\hat{H}_{23}\hat{H}_{41}}\right)\left(\frac{\left(\hat{H}_{43}\Delta H_{21}-\hat{H}_{41}\Delta H_{23}\right)X_2}{\hat{H}_{43}\hat{H}_{21}-\hat{H}_{23}\hat{H}_{41}}\right)^{*}\right]\\&+\mathbb{E}\left[\left(\frac{\left(\hat{H}_{43}\Delta H_{41}-\hat{H}_{41}\Delta H_{43}\right)X_4}{\hat{H}_{43}\hat{H}_{21}-\hat{H}_{23}\hat{H}_{41}}\right)\left(\frac{\left(\hat{H}_{43}\Delta H_{41}-\hat{H}_{41}\Delta H_{43}\right)X_4}{\hat{H}_{43}\hat{H}_{21}-\hat{H}_{23}\hat{H}_{41}}\right)^{*}\right]\\=&\frac{\mathbb{E}\left[|X_2|^2\right]\left(|H_{43}|^2\mathbb{E}\left[|\Delta H_{21}|^2\right]+|H_{41}|^2\mathbb{E}\left[|\Delta H_{23}|^2\right]\right)}{|H_{43}H_{21}-H_{23}H_{41}|^2}+\frac{\mathbb{E}\left[|X_4|^2\right]\left(|H_{43}|^2\mathbb{E}\left[|\Delta H_{41}|^2\right]+|H_{41}|^2\mathbb{E}\left[|\Delta H_{43}|^2\right]\right)}{|H_{43}H_{21}-H_{23}H_{41}|^2}\\=&\frac{\sigma^2}{(N_T-1)}\frac{|H_{43}|^2+|H_{41}|^2}{|H_{43}H_{21}-H_{23}H_{41}|^2}.\end{aligned} \tag{93}$$

$$\mathbb{V}[E_W]=\mathbb{E}\left[|E_W|^2\right]=\mathbb{E}\left[\left(\frac{\hat{H}_{43}W_1-\hat{H}_{41}W_3}{\hat{H}_{43}\hat{H}_{21}-\hat{H}_{23}\hat{H}_{41}}\right)\left(\frac{\hat{H}_{43}W_1-\hat{H}_{41}W_3}{\hat{H}_{43}\hat{H}_{21}-\hat{H}_{23}\hat{H}_{41}}\right)^{*}\right]=\frac{|H_{43}|^2\sigma^2+|H_{41}|^2\sigma^2}{|H_{43}H_{21}-H_{23}H_{41}|^2}. \tag{94}$$

$$\mathbb{V}[\Delta X_2]=\mathbb{V}[E_{SI}]+\mathbb{V}[E_{SOI}]+\mathbb{V}[E_W]=\sigma^2\frac{|H_{43}|^2+|H_{41}|^2}{|H_{43}H_{21}-H_{23}H_{41}|^2}\left(\frac{2}{N_T-1}+1\right). \tag{95}$$

channel estimation procedure is the same as in SISO IBFD, thus all channel estimation errors are i.i.d RVs with $\Delta H_{ij} \sim \mathcal{CN}(0, \frac{\sigma^2}{N_T E_S})$. Similarly to SISO IBFD, the RV ΔX_2 is the sum of independent RVs with zero mean. Thus, the variance of ΔX_2 can be expressed as

$$\mathbb{V}[\Delta X_2] = \mathbb{V}[E_{SI}] + \mathbb{V}[E_{SOI}] + \mathbb{V}[E_W]. \tag{83}$$

The variances of the all components can be computed as

$$\begin{aligned}
\mathbb{V}[E_{SI}] &= \mathbb{E}\Big[|E_{SI}|^2\Big] \\
&= \mathbb{E}\left[\frac{\Delta H_{11}\hat{H}_{21}^* + \Delta H_{13}\hat{H}_{23}^*}{\left|\hat{H}_{21}\right|^2 + \left|\hat{H}_{23}\right|^2} X_1 \left(\frac{\Delta H_{11}\hat{H}_{21}^* + \Delta H_{13}\hat{H}_{23}^*}{\left|\hat{H}_{21}\right|^2 + \left|\hat{H}_{23}\right|^2} X_1\right)^*\right] \\
&= \frac{\mathbb{E}\big[|X_1|^2\big]\big(\mathbb{E}\big[|\Delta H_{11}|^2\big]|H_{21}|^2 + \mathbb{E}\big[|\Delta H_{13}|^2\big]|H_{23}|^2\big)}{\big(|H_{21}|^2 + |H_{23}|^2\big)^2} \\
&= \frac{\sigma^2}{N_T\big(|H_{21}|^2 + |H_{23}|^2\big)},
\end{aligned} \tag{84}$$

$$\begin{aligned}
\mathbb{V}[E_{SOI}] &= \mathbb{E}\Big[|E_{SOI}|^2\Big] \\
&= \mathbb{E}\left[\frac{\Delta H_{21}\hat{H}_{21}^* + \Delta H_{23}\hat{H}_{23}^*}{\left|\hat{H}_{21}\right|^2 + \left|\hat{H}_{23}\right|^2} X_2 \left(\frac{\Delta H_{21}\hat{H}_{21}^* + \Delta H_{23}\hat{H}_{23}^*}{\left|\hat{H}_{21}\right|^2 + \left|\hat{H}_{23}\right|^2} X_2\right)^*\right] \\
&= \frac{\mathbb{E}\big[|X_2|^2\big]\big(\mathbb{E}\big[|\Delta H_{21}|^2\big]|H_{21}|^2 + \mathbb{E}\big[|\Delta H_{23}|^2\big]|H_{23}|^2\big)}{\big(|H_{21}|^2 + |H_{23}|^2\big)^2} \\
&= \frac{\sigma^2}{N_T\big(|H_{21}|^2 + |H_{23}|^2\big)},
\end{aligned} \tag{85}$$

$$\begin{aligned}
\mathbb{V}[E_W] &= \mathbb{E}\Big[|E_W|^2\Big] \\
&= \mathbb{E}\left[\left(\frac{W_1\hat{H}_{21}^* + W_3\hat{H}_{23}^*}{\left|\hat{H}_{21}\right|^2 + \left|\hat{H}_{23}\right|^2}\right)\left(\frac{W_1\hat{H}_{21}^* + W_3\hat{H}_{23}^*}{\left|\hat{H}_{21}\right|^2 + \left|\hat{H}_{23}\right|^2}\right)^*\right] \\
&= \frac{\sigma^2|H_{21}|^2 + \sigma^2|H_{23}|^2}{\big(|H_{21}|^2 + |H_{23}|^2\big)^2} = \frac{\sigma^2}{|H_{21}|^2 + |H_{23}|^2}.
\end{aligned} \tag{86}$$

Finally, the variance of ΔX_2 in SIMO IBFD yields

$$\mathbb{V}[\Delta X_2] = \frac{\sigma^2}{|H_{21}|^2 + |H_{23}|^2}\left(\frac{2}{N_T} + 1\right). \tag{87}$$

D. ERROR VECTOR VARIANCE IN MIMO IBFD

We compute the variance of ΔX_2 in MIMO IBFD given by (81). For channel estimation in MIMO, the orthogonal symbols are used as defined in Table 1 and the available power E_S is equally shared between two transmitters. From (11)-(14), we can determine the SI channel estimation errors ΔH_{11}, ΔH_{13}, ΔH_{31}, and ΔH_{33} as

$$\begin{bmatrix} \hat{H}_{11}^{(l)} & \hat{H}_{31}^{(l)} \\ \hat{H}_{13}^{(l)} & \hat{H}_{33}^{(l)} \end{bmatrix} = \begin{bmatrix} H_{11} & H_{31} \\ H_{13} & H_{33} \end{bmatrix} + \begin{bmatrix} W_1^{(l-1)} & W_1^{(l)} \\ W_3^{(l-1)} & W_3^{(l)} \end{bmatrix} \begin{bmatrix} X_1^{(l-1)} & X_1^{(l)} \\ X_3^{(l-1)} & X_3^{(l)} \end{bmatrix}^{-1}, \tag{88}$$

$$\begin{bmatrix} \Delta H_{11}^{(l)} & \Delta H_{31}^{(l)} \\ \Delta H_{13}^{(l)} & \Delta H_{33}^{(l)} \end{bmatrix} = -\begin{bmatrix} W_1^{(l-1)} & W_1^{(l)} \\ W_3^{(l-1)} & W_3^{(l)} \end{bmatrix} \begin{bmatrix} X_1^{(l-1)} & X_1^{(l)} \\ X_3^{(l-1)} & X_3^{(l)} \end{bmatrix}^{-1}, \tag{89}$$

$$\begin{bmatrix} \Delta H_{11} & \Delta H_{31} \\ \Delta H_{13} & \Delta H_{33} \end{bmatrix} = \frac{1}{N_T - 1} \sum_{l=1}^{N_T - 1} \begin{bmatrix} \Delta H_{11}^{(l)} & \Delta H_{31}^{(l)} \\ \Delta H_{13}^{(l)} & \Delta H_{33}^{(l)} \end{bmatrix}. \tag{90}$$

Using $N_T - 1$ training symbols ($N_T \geq 2$), the variances of the SI and SOI channel estimation errors equal

$$\mathbb{V}[\Delta H_{SI}] = \frac{\sigma^2}{(N_T - 1)E_S}, \ \mathbb{V}[\Delta H_{SOI}] = \frac{\sigma^2}{(N_T - 1)E_S}, \tag{91}$$

where ΔH_{SI} represents ΔH_{11}, ΔH_{13}, ΔH_{31}, or ΔH_{33}, and ΔH_{SOI} represents ΔH_{21}, ΔH_{41}, ΔH_{23}, or ΔH_{43}.

Lastly, the variance of ΔX_2 is determined in (92)-(95), shown at the bottom of the previous page.

REFERENCES

[1] A. Sabharwal, P. Schniter, D. Guo, D. W. Bliss, S. Rangarajan, and R. Wichman, "In-band full-duplex wireless: Challenges and opportunities," *IEEE J. Sel. Areas Commun.*, vol. 32, no. 9, pp. 1637–1652, Sep. 2014.

[2] Z. Zhang, K. Long, A. V. Vasilakos, and L. Hanzo, "Full-duplex wireless communications: Challenges, solutions, and future research directions," *Proc. IEEE*, vol. 104, no. 7, pp. 1369–1409, Jul. 2016.

[3] G. Prasad, L. Lampe, and S. Shekhar, "Enhancing transmission efficiency of broadband PLC systems with in-band full duplexing," in *Proc. Int. Symp. Power Line Commun. Appl.*, 2016, pp. 46–51.

[4] J. Zhang, H. Luo, N. Garg, A. Bishnu, M. Holm, and T. Ratnarajah, "Design and analysis of wideband in-band-full-duplex FR2-IAB networks," *IEEE Trans. Wireless Commun.*, vol. 21, no. 6, pp. 4183–4196, Jun. 2022.

[5] F. Passerini and A. M. Tonello, "In band full duplex PLC: The role of the hybrid coupler," in *Proc. Int. Symp. Power Line Commun. Appl. (ISPLC)*, 2016, pp. 52–57.

[6] F. Passerini and A. M. Tonello, "Adaptive hybrid circuit for enhanced echo cancellation in full duplex PLC," in *Proc. IEEE Int. Symp. Power Line Commun. Appl. (ISPLC)*, 2018, pp. 1–5.

[7] D. Righini and A. M. Tonello, "MIMO in-band-full-duplex PLC: Design, analysis and first hardware Realization of the analog self-interference cancellation stage," *IEEE Open J. Comm. Soc.*, vol. 2, pp. 1344–1357, 2021.

[8] G. Prasad, L. Lampe, and S. Shekhar, "In-band full duplex broadband power line communications," *IEEE Trans. Commun.*, vol. 64, no. 9, pp. 3915–3931, Sep. 2016.

[9] G. Prasad, L. Lampe, and S. Shekhar, "Digitally controlled analog cancellation for full duplex broadband power line communications," *IEEE Trans. Commun.*, vol. 65, no. 10, pp. 4419–4432, Oct. 2017.

[10] F. J. C. Corripio, J. A. C. Arrabal, L. D. del Rio, and J. T. E. Munoz, "Analysis of the cyclic short-term variation of indoor power line channels," *IEEE J. Sel. Areas Commun.*, vol. 24, no. 7, pp. 1327–1338, Jul. 2006.

[11] S. Katar, B. Mashburn, K. Afkhamie, H. Latchman, and R. Newman, "Channel adaptation based on cyclo-stationary noise characteristics in PLC systems," in *Proc. IEEE Int. Symp. Power Line Commun. Appl.*, 2006, pp. 16–21.

[12] V. Korzhun and A. M. Tonello, "Pilot-free channel tracking for in-band full-duplex broadband power line communications," in *Proc. IEEE Int. Symp. Power Line Commun. Appl.*, 2021, pp. 37–42.

[13] V. Korzhun and A. M. Tonello, "Achievable throughput in in-band full-duplex broadband power line communications," in *Proc. IEEE Int. Symp. Power Line Commun. Appl.*, 2023, pp. 49–54.

[14] C. Nam, C. Joo, and S. Bahk, "Joint subcarrier assignment and power allocation in full-duplex OFDMA networks," *IEEE Trans. Wireless Commun.*, vol. 14, no. 6, pp. 3108–3119, Jun. 2015.

[15] Z. Tong and M. Haenggi, "Throughput analysis for full-duplex wireless networks with imperfect self-interference cancellation," *IEEE Trans. Commun.*, vol. 63, no. 11, pp. 4490–4500, Nov. 2015.

[16] J. Marašević, J. Zhou, H. Krishnaswamy, Y. Zhong, and G. Zussman, "Resource allocation and rate gains in practical full-duplex systems," *IEEE/ACM Trans. Netw.*, vol. 25, no. 1, pp. 292–305, Feb. 2017.

[17] *Unified High-Speed Wire-Line Based Home Networking Transceivers–Power Spectral Density Specification*, ITU-Rec. G.9964, Int. Telecommun. Union, Geneva, Switzerland, 2011. [Online]. Available: http://handle.itu.int/11.1002/1000/11406

[18] T. Esmailian, F. R. Kschischang, and P. Glenn Gulak, "In-building power lines as high-speed communication channels: Channel characterization and a test channel ensemble," *Int. J. Commun. Syst.*, vol. 16, no. 5, pp. 381–400, 2003. [Online]. Available: https://onlinelibrary.wiley.com/doi/abs/10.1002/dac.596

[19] L. Di Bert, P. Caldera, D. Schwingshackl, and A. M. Tonello, "On noise modeling for power line communications," in *Proc. IEEE Int. Symp. Power Line Commun. Appl.*, 2011, pp. 283–288.

[20] A. Garcia Armada, "SNR gap approximation for M-PSK-based bit loading," *IEEE Trans. Wireless Commun.*, vol. 5, no. 1, pp. 57–60, Jan. 2006.
[21] S. D'Alessandro, A. M. Tonello, and L. Lampe, "Bit-loading algorithms for OFDM with adaptive cyclic prefix length in PLC channels," in *Proc. IEEE Int. Symp. Power Line Commun. Appl.*, 2009, pp. 177–181.
[22] D. Yoon, K. Cho, and J. Lee, "Bit error probability of M-ary quadrature amplitude modulation," in *Proc. Veh. Technol. Conf. Fall IEEE VTS Fall VTC 52nd Veh. Technol. Conf.*, 2000, pp. 2422–2427.
[23] G. Proakis, *Digital Communications 5th Edition*. New York, NY, USA: McGraw Hill, 2007.
[24] *Unified High-Speed Wire-Line Based Home Networking Transceivers–System Architecture and Physical Layer Specification*, ITU-Rec. G.9960, Int. Telecommun. Union, Geneva, Switzerland, 2018. [Online]. Available: http://handle.itu.int/11.1002/1000/13775

VITALI KORZHUN (Graduate Student Member, IEEE) received the Dipl.Ing. and M.Sc. degrees in electrical engineering from the Belarusian State University of Informatics and Radioelectronics, Belarus, in 2013 and 2016, respectively. He is currently pursuing the Ph.D. degree in information and communication engineering with the University of Klagenfurt. In 2019, he joined the University of Klagenfurt, Austria, as a Research and Teaching Assistant. His research interests include signal processing, power line communications, and in-band full-duplex communication.

ANDREA M. TONELLO (Senior Member, IEEE) received the Laurea degree (summa cum laude) in electrical engineering and the Ph.D. degree in electronics and telecommunications from the University of Padova, Padua, Italy, in 1996 and 2002, respectively. From 1997 to 2002, he was with Bell Labs-Lucent Technologies, Whippany, NJ, USA, first as a member of the Technical Staff. He was then promoted to a Technical Manager and appointed as the Managing Director of the Bell Labs, Italy Division. In 2003, he joined the University of Udine, Udine, Italy, where he became an Aggregate Professor in 2005, and an Associate Professor in 2014. He is currently a Professor with the Chair of Embedded Communication Systems, University of Klagenfurt, Klagenfurt, Austria. He also has a post as a part-time Associate Professor with the University of Udine. He received several awards, including the Bell Labs Recognition of Excellence Award in 1999, the Distinguished Visiting Fellowship from the Royal Academy of Engineering, U.K., in 2010, the IEEE Distinguished Lecturer Award from VTS from 2011 to 2015, and from COMSOC from 2018 to 2019, the Italian Full Professor Habilitation in 2013, and the Chair of Excellence from Carlos III Universidad, Madrid, from 2019 to 2020. He was also a co-recipient of ten best paper awards. He serves/served as an Associate Editor for several journals, including IEEE TRANSACTIONS ON VEHICULAR TECHNOLOGY, IEEE TRANSACTIONS ON COMMUNICATIONS, IEEE ACCESS, and *IET Smart Grid*. He was the general chair or the TPC co-chair of several conferences. He was the Chair of the IEEE COMSOC Technical Committee on Power Line Communications from 2014 to 2018 and the Chair of the TC on Smart Grid Communications from 2020 to 2023. He also served as the Director of Industry Outreach of IEEE COMSOC from 2019 to 2020.